

Design and Implementation of a Wireless Charger

ECE 4600 - Final Report

Prepared By:

Mario Phaneuf

Oliver Bloch

Ryan Kostynuik

Ryan Officer

Tim Beck

Department of Electrical and Computer Engineering

University of Manitoba

Winnipeg, Manitoba, Canada

March 17th, 2017

©2017 Mario Phaneuf, Oliver Bloch, Ryan Kostynuik, Ryan Officer, Tim Beck

Abstract

Wireless charging systems have emerged in recent years as a solution to the endless number of cables required to power household devices. These systems rely on the concept of resonant power transfer to eliminate the need for wires. The goal of this project was to design and build a practical and efficient wireless cellphone charger as a demonstration of the capabilities of this concept.

The final design consisted of a primary and secondary circuit interfaced via 2 coupled planar surface coils. The primary side circuit consisted of a 3 stage AC-AC converter responsible for supplying power to a primary source coil. Mains voltage, 120VAC at 60Hz, was supplied to a rectifier circuit which was stepped down to 12VDC. Following the rectifier circuit was an inverter which converted the 12VDC voltage to 12VAC at variable high frequency, on the order of 10^5 Hz. An Arduino UNO controlled the inverter switches via gate driver integrated circuits. The microcontroller also managed the radio frequency identification phone recognition system. The high frequency voltage was applied to the primary coil which induced a high-frequency magnetic field perpendicularly aligned to the surface of the secondary coil. The high frequency magnetic field induced an AC voltage on the secondary coil. The secondary circuit rectified and regulated the induced voltage to 5VDC. In the final build, the primary electronics were housed in a 3D printed charging pad and the secondary electronics were housed in a 3D printed phone case. An RFID circuit between the pad and the phone case controlled operation of the charger. During the absence of the phone, the inverter did not operate and no power was output. In the presence of the phone, the circuit would be completed and the phone would successfully charge.

Four specifications were outlined for this project: input voltage, output voltage, output current and efficiency. Testing revealed that the circuit met all specifications with the exception of efficiency. The maximum efficiency achieved was 36% at an inverter switching frequency of 33kHz. The output voltage was regulated to 5VDC to comply with the USB standard. At this voltage the design had the capability to supply 1.5A. Although the target efficiency was not achieved, a functional wireless cellphone charger was successfully produced.

Acknowledgments

The authors of this report would like to thank the following people for their contributions and support. Without their contributions, the completion of this project would not have been possible.

- Carl Ho, Ph.D., P. Eng
- Derek Oliver, Ph.D.
- Ahmad Byagowi, Ph.D., P. Eng
- Daniel Card, P. Eng
- Aidan Topping
- Zoran Trajkoski
- Sinisa Janjic

Division of Work

	<i>Tim Beck</i>	<i>Ryan Officer</i>	<i>Ryan Kostyniuk</i>	<i>Oliver Bloch</i>	<i>Mario Phaneuf</i>
<i>Project Proposal</i>	●	○	●	○	○
<i>Design Review #2</i>		●		●	
<i>Design Review #3</i>					●
<i>Design Review #4</i>	●		●		
<i>Primary Rectifier Simulation and Selection</i>					●
<i>Inverter Simulation and Design</i>	○		●		
<i>Inverter Switching and Peripheral Controls</i>			●		
<i>Planar Inductive Coil Simulation and Selection</i>	●				
<i>Secondary Rectifier and Regulator Design</i>					●
<i>Case Design and Printing</i>		●			●
<i>Integration</i>	●		●		
<i>Final Report Writing</i>	●	●	●	●	●
<i>Final Report Compilation</i>					●

● = Primary Contribution

○ = Secondary Contribution

Table of Contents

Abstract	i
Acknowledgments	ii
Division of Work	iii
Table of Contents	iv
List of Figures	vi
List of Tables	vii
Nomenclature	viii
1 Introduction	1
2 Planar Surface Coils	2
2.1 Equivalent Coupled Coil Model	2
2.1.1 Model Confirmation	3
2.2 Model Values	4
2.2.1 Coil Selection	4
2.2.2 Coupling Coefficient	5
2.3 Resonant Circuit	7
2.4 Protection	8
3 Primary AC-DC Converter	9
3.1 Single Phase Bridge Rectifier	9
3.1.1 Initial Design	11
3.2 Buck Converter	12
3.2.1 Initial Design	12
3.3 Reactive Power Compensation	14
3.4 Circuit Efficiency Considerations	14
3.5 Simulation and Results	15
3.5.1 Physical Implementation	18
3.5.2 Testing & Results	20
4 Arduino	20
4.1 General Overview	21
4.2 Cell Phone Detection Module	22
4.2.1 Design Considerations	22
4.2.2 Implementation	23
4.3 Inverter Signal Generation	23
4.3.1 Design Considerations	24
4.3.2 Implementation	24
5 Inverter	26
5.1 Design Considerations	26
5.2 MOSFETS	27
5.3 H-Bridge	28
5.3.1 Initial Simulation	29
5.3.2 Second Simulation	30
5.3.3 Third Simulation	30
5.4 Driving The H-Bridge	31

5.4.1	Pulse Transformers	31
5.4.2	Gate Drivers	31
5.4.3	NOT Circuit	32
5.5	Building the Inverter	33
5.5.1	H-Bridge MOSFET and Wire Selection	33
5.5.2	Gate Driver Selection	34
5.5.3	DC-DC Converter	35
5.6	Operation Results of Inverter - No Coupling	36
6	Secondary Circuit	37
6.1	Voltage Rectification	37
6.2	Voltage Regulation	38
6.2.1	Input Voltage Requirements	39
6.3	Transient Voltage Suppression	40
6.4	Phone Integration	40
6.5	Implementation	42
7	Case Design	43
7.1	Design Considerations	43
7.2	Implementation	44
8	Final Design	44
8.1	System Integration	45
8.2	Operation Results	47
8.3	Analysis of Results	48
8.3.1	Achievement of Specifications	48
8.3.2	Efficiency Analysis	48
9	Future Considerations	50
10	Conclusion	50
Appendix A - Coil Model Derivation		52
Appendix B - Complete Circuit		55
Appendix C - Arduino		56
Appendix D - Budget		59
Appendix E - Secondary Circuit Rectifier Efficiency		60
Bibliography		62

List of Figures

1.1	Wireless cellphone charger block diagram.	1
2.1	Coupled inductor equivalent circuit model.	3
2.2	Multisim simulation for verification of planar surface coil model.	4
2.3	Input current Multisim simulation results.	5
2.4	Coupling coefficient factor versus displacement.	6
2.5	AC analysis for coupled coils and resistive load.	7
2.6	AC analysis for resonant coupled coils and resistive load.	7
2.7	Shielding effectiveness for ferrite and copper layers.	8
3.1	Full wave bridge rectifier schematic.	10
3.2	Full wave bridge rectifier waveform.	10
3.3	Full bridge rectifier initial design.	12
3.4	Buck converter schematic.	12
3.5	Buck converter initial design.	13
3.6	Full bridge rectifier with smoothing inductor.	15
3.7	Two stage AC-DC converter voltage waveforms.	16
3.8	Two stage AC-DC converter output.	17
3.9	AC-DC converter inrush current requirements.	20
4.1	Arduino control process.	21
4.2	Control circuit wiring diagram.	23
4.3	Gate driver signals.	25
5.1	Current path for H-Bridge Inverter.	28
5.2	The inverter circuit.	29
5.3	The simulated inverter voltage and current output	30
5.4	The gate driver output.	32
5.5	The NOT circuit.	33
5.6	Inverter output waveform at 30kHz.	36
5.7	Inverter output waveform at 160kHz.	36
6.1	Output voltage of full-circuit simulation.	38
6.2	Dedicated charging port diagram.	41
6.3	Secondary circuit output.	42
7.1	3D Model of phone case.	44
8.1	Successful wireless charging at 1200mA.	45
8.2	Implemented system with 3.3Ω load.	46
8.3	Implemented system successfully charging a Samsung Galaxy S4.	46

List of Tables

1.1	Project target specifications.	2
3.1	AC-DC power supply technical specifications.	19
5.1	MOSFET parameters.	34
5.2	Gate driver technical specifications.	34
6.1	CUI voltage regulator technical specifications.	39
6.2	Dedicated charging port specifications.	41
8.1	Efficiency results with coupling coefficient of 0.8.	47
8.2	Efficiency results with coupling coefficient of 0.6.	48
8.3	Achieved project specifications.	48

Nomenclature

Abbreviation	Description
IC	Integrated Circuit
RFID	Radio Frequency Identification
PCB	Printed Circuit Board
Q	Quality Factor
EMI	Electromagnetic Interference
SE	Shielding Effectiveness
ESR	Equivalent Series Resistance
RMS	Root Mean Square
MOSFET	Metal Oxide Semiconductor Field Effect Transistor
PWM	Pulse Width Modulation
μ	Permittivity
η	Efficiency

1 Introduction

The goal of this project was to design and implement a wireless cell phone charger. The charger relies on the concept of resonant power transfer to be able to transmit wireless power. The project design is based on the paper entitled “Design and Implementation of a Low-Profile Contactless Battery Charger Using Planar Printed Circuit Board Windings as Energy Transfer Device” which details a conceptual design for the wireless power transfer circuit [1].

The final design consisted of a primary and secondary circuit interfaced via 2 coupled planar surface coils. The primary side circuit consisted of a 3 stage AC-AC converter responsible for supplying power to a primary source coil. Mains voltage, 120VAC at 60Hz, was supplied to a rectifier circuit which was stepped down to 12VDC. Following the rectifier circuit was an inverter which converted the 12VDC voltage to 12VAC at variable high frequency, on the order of 10^5 Hz. An Arduino UNO controlled the inverter switches via gate driver integrated circuits (IC). The microcontroller also managed the radio frequency identification phone (RFID) recognition system. The high frequency voltage was applied to the primary coil which induced a high-frequency magnetic field perpendicularly aligned to the surface of the secondary coil. The entire primary circuit was enclosed in a 3D printed case. The high frequency magnetic field induced an AC voltage on the secondary coil. The secondary circuit rectified and regulated the induced voltage to 5VDC. The secondary circuit was housed in a 3D printed case specific to a Samsung Galaxy S4 and was connected via Micro-B cable. Figure 1.1 shows a block diagram of the complete project.

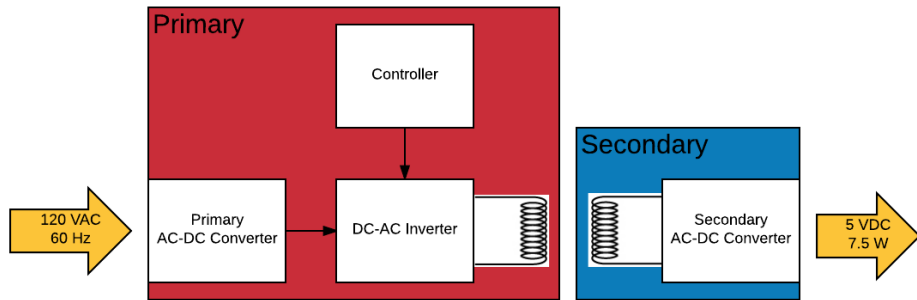


Figure 1.1: Wireless cellphone charger block diagram.

A 3D printed charging pad housed the primary electronics and RFID transmitter which allowed for optimal coupling of the coils and alignment with the RFID tag. A 3D printed phone case housed the secondary electronics. The RFID circuit ensured that the inverter did not operate in the absence of the device.

The success of the project was tied to four proposed specifications. The specifications refer to target input and output voltages, input current, and efficiency. Above all else, the demonstration of a functional wireless cellphone charger would be considered a success. The project specification targets are listed in Table 1.1 below.

Table 1.1: Project target specifications.

Performance Metric	Target Value
Input Voltage	120VAC, 60Hz
Output Voltage	5VDC Nominal, 4.75-5.25VDC Range
Output Current	0.5 - 1.5A
Efficiency	55% Nominal Max

The output current specification refers only to the current capacity of the wireless charger, not the actual current drawn by the Samsung S4. It was therefore sufficient to show the output capabilities of the charger with a resistive load. Efficiency can also be measured with respect to a resistive load.

2 Planar Surface Coils

The wireless power transfer capabilities between two planar surface coils is the founding principle of this project. Initially, these coils were to be designed and manufactured on a Printed Circuit Board (PCB). However, design requirements of the surrounding power electronics stipulated the need for an accurate coil model early in the design process. In addition, coil inductance values would be difficult to obtain without first building the coils. The workaround to this problem was to simply purchase the coils. This chapter will cover the coupled coil model, the selection of appropriate coils, and protection.

2.1 Equivalent Coupled Coil Model

In order to proceed with design of primary and secondary power electronic circuits, an equivalent circuit model of the planar surface coils was required. Figure 2.1 shows an equivalent circuit model of the planar source coils that was used for all simulations. L_{11} and L_{22} are the self inductances of the coils and L_M is the mutual inductance. Derivation of said model can be found in Appendix A.

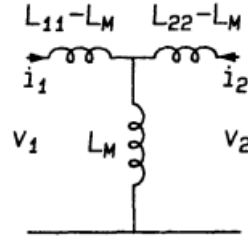


Figure 2.1: Coupled inductor equivalent circuit model [2].

The coupling coefficient, k , of two coupled inductors is the ratio defining the amount of primary coil flux that passes through the secondary coil and vice versa. This can be related to the values in the coupled coil model by Equation 2.1 [2].

$$k = \frac{L_M}{\sqrt{L_{11}L_{22}}} \quad (2.1)$$

Assuming each coil has the same self inductance, $L_{11} = L_{22} = L$, then the mutual inductance can be found as:

$$kL = L_M \quad (2.2)$$

If the coupling coefficient and the inductance of the individual coils are known, the mutual inductance can be found and an accurate model of the planar surface coils can be formed.

2.1.1 Model Confirmation

Once the coupled coil model was determined, it required verification which was accomplished using Multisim. This software was selected for its coupled inductor component model, which could provide a direct side-by-side comparison to a simulation of the coil model derived in Appendix A. It should be noted that this Multisim simulation was simply for verification purposes and full design simulations were completed in PLECS.

The circuit simulations were completed at a frequency of 500kHz, with a $10V_{rms}$ source voltage and a 3.3Ω resistive load. The source current and load current were measured and compared to verify the derived model's accuracy. Figure 2.2 (a) shows the simulated results when using the coupled inductor component, while Figure 2.2 (b) shows the simulated results when the derived circuit model was used.

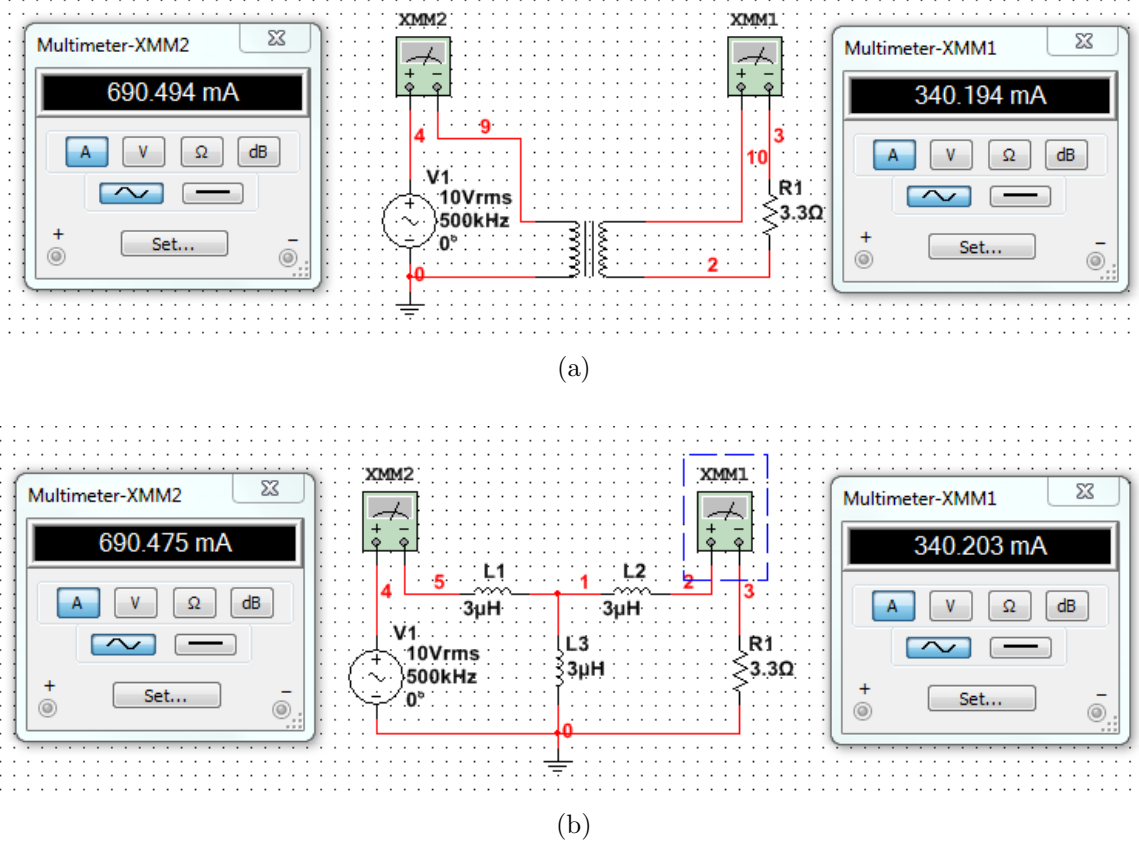


Figure 2.2: Multisim simulation for verification of planar surface coil model. (a) Multisim coupled inductor component. (b) Coupled inductor equivalent circuit model.

Results shown in Figure 2.2 (a) and Figure 2.2 (b) share four significant figures of precision which validated the accuracy of the derived equivalent circuit model.

2.2 Model Values

To complete the equivalent model, physical coils had to be specified to obtain the inductance values and the coupling coefficient k had to be estimated.

2.2.1 Coil Selection

The selection of an appropriate set of coils was based on three parameters: the current rating, resistance and physical dimensions of the coil.

The required current capability was estimated through simulations of the derived circuit model. This circuit was simulated with a 10V_{rms}, 150kHz source supplying a load of

3.3Ω through the coupled coils. A 3.3Ω load was chosen specifically to simulate a 5VDC, 7.5W load requirement. A coupling coefficient of 0.6 was selected for the model which is justified in Section 2.2.2. $6\mu\text{H}$ coils were found to be common and were therefore used in the circuit model. A series capacitor was added to introduce resonance, a topic to be discussed in further detail in Section 2.3. The simulated circuit and results can be seen in Figure 2.3.

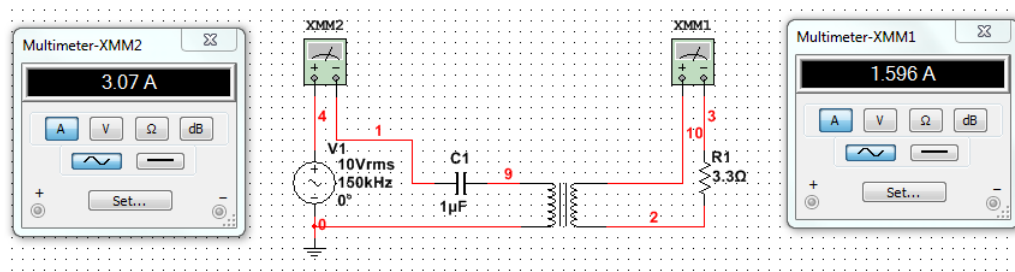


Figure 2.3: Input current Multisim simulation results.

In order to supply 7.5W in a lossless circuit, the required source current was 3A. Given a target efficiency of 55% and a safety margin of 2A, the current rating was chosen to be 8A.

The next important coil characteristic was the size. With plans to enclose the receiving coil within the phone case, the coil could not be larger than the maximum dimensions of the phone. The Samsung Galaxy S4 was selected as the mobile device and so the coil diameter had to be limited to 50mm. To increase the amount of flux captured, the coil diameter was maximized within this constraint.

The third and final coil characteristic considered was the coil resistance, which would have a direct effect on the final circuit efficiency. The coil resistance at higher frequencies is related to the quality factor (Q) of the coil by the following equation:

$$Q = \frac{X_L}{R} = \frac{\omega L}{R} \quad (2.3)$$

The selected coil should have a large Q for a given inductance value L .

A Wurth Electronics planar surface coil proved to be the best option while meeting the aforementioned criteria [3].

2.2.2 Coupling Coefficient

With the self-inductance of the coils known, the equivalent coupled coil model only needed a coupling coefficient in order to complete the model to be used in a full

circuit simulation. The coupling coefficient would have an effect on overall circuit efficiency and thus an accurate value was required to obtain realistic circuit simulations. In general, the coupling coefficient varies with coil displacement; k increases as displacement between coils decreases, and vice versa. To obtain the true coupling coefficient as a function of displacement, measurements with the physical coils would need to be taken.

In the initial design stage an estimate for the coupling coefficient was needed before it could be measured. Coupling factor data for 30mm coils was found and was considered an accurate estimate for the behaviour of the 50mm coils. Based off of this coupling factor data, shown in Figure 2.4, the coupling coefficient estimate was set at 0.6¹. This corresponds to a 2.5mm air gap, which was considered appropriate for physical implementation.

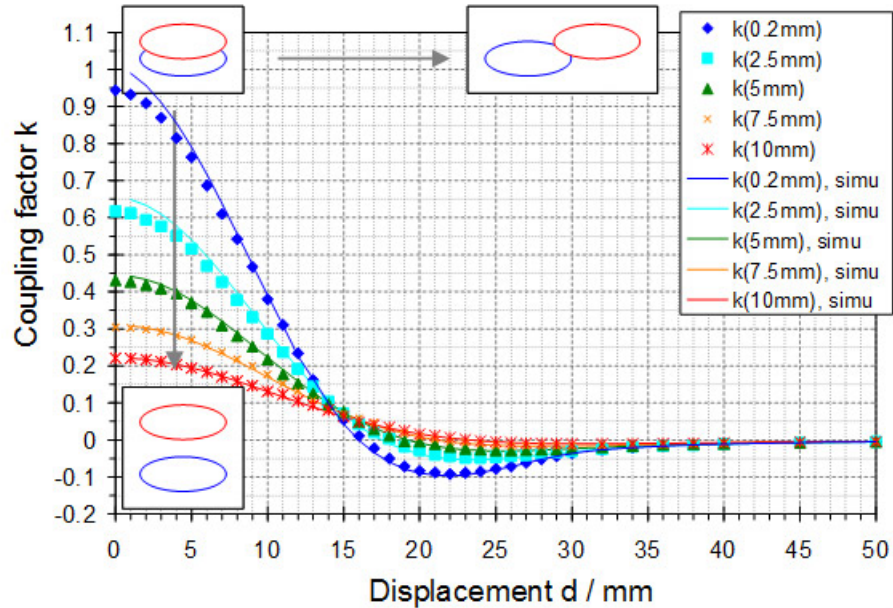


Figure 2.4: Coupling coefficient factor versus displacement.

After the coils were purchased and received, the coupling coefficient was measured. Previous simulations showed that the coupled coils behaved like a 1: k transformer, where k is the coupling coefficient. By this property it was determined that when the coils were overlaid on top of each other, the coupling coefficient was approximately 0.8. A coupling coefficient of 0.6 occurred when there was a 2mm air gap, instead of the expected 2.5mm. However, a 2mm air gap was still considered physically achievable.

¹<https://www.wirelesspowerconsortium.com/technology/coupling-factor.html>

2.3 Resonant Circuit

As reactive elements, the coupled coils exhibit a particular frequency response. This response can be likened to a bandpass filter with low gain and a wide bandwidth. To illustrate this, a frequency sweep was performed for the coupled coils, with $k = 0.6$, and a 3.3Ω resistive load. The results of this sweep are shown Figure 2.5 below, with the frequency axis on a logarithmic scale.

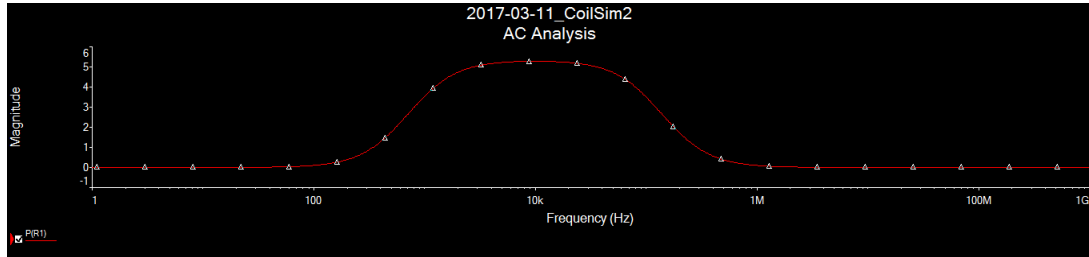


Figure 2.5: AC analysis for coupled coils and resistive load.

The power delivered to the 3.3Ω load is approximately 5W over the passband. The wireless charger needs to be able to supply 7.5W, and thus the coils by themselves would not be able to transfer the power required by this project.

By introducing a series capacitor to the coupled coils, the frequency response changed from the bandpass response shown in Figure 2.5 to a resonant response shown in Figure 2.6.

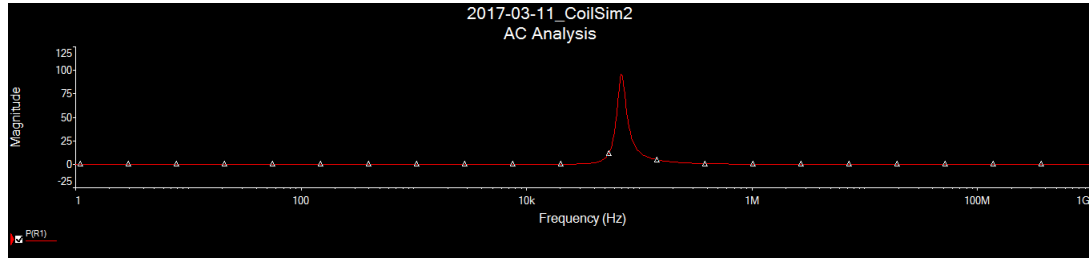


Figure 2.6: AC analysis for resonant coupled coils and resistive load.

There is a distinct difference between the two responses. In the resonant case, there are two different frequencies which delivered sufficient power. Additionally, in practice the frequency could be tuned to account for varying coupling coefficients and non ideal circuit qualities.

The resonant frequency response is not symmetric and so it can be inferred that one of the frequencies will yield better results. Using the plot in Figure 2.6, the two target

frequencies were found to be 48kHz and 137kHz. A single frequency simulation at 48kHz required 8.356W from the source to supply 7.557W to the load. This gives an efficiency of $7.556/8.356 = 90.4\%$. On the other hand, the single frequency simulation at 137kHz provided an efficiency of $7.325/7.619 = 96.1\%$. It would be preferable to operate the inverter at the higher frequency so that the coupled coil efficiency is maximized.

2.4 Protection

Early in the design process, concerns were raised about the effect of the magnetic field on the phone. The main concern was that it would be adversely affected and potentially damaged. The secondary concern was that the presence of Eddy currents would hurt the efficiency.

The solution to the first concern is the introduction of an electromagnetic interference (EMI) shield. An EMI shield is any kind of physical barrier which inhibits the magnetic field from penetrating it. The shield can be made of a metallic or a magnetic material. The strength of the shielding material is given by the shielding effectiveness (SE), which is defined as the ratio of the penetrating field with the shield present and the penetrating field without the shield present. A plot of the shielding effectiveness for a layer of ferrite and a layer of copper is shown in Figure 2.7 ².

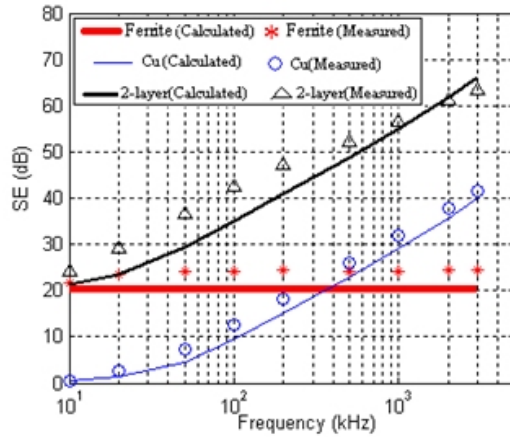


Figure 2.7: Shielding effectiveness for ferrite and copper layers.

A layer of ferrite achieves a constant SE across relevant wireless charging frequencies. A layer of copper has an SE which increases with frequency. Either material can be used individually or they can be combined as needed. If both a ferrite and copper sheet are

²<https://www.wirelesspowerconsortium.com/technology/shielding-effectiveness.html>

used, the SE at 100kHz is approximately 35dB. This would ensure that the power shielding would be 70dB, or that the power of the shielded field would be 10 million times smaller than the power of the incident wave. Even with just a copper sheet the power shielding would be 20dB. It was not initially clear if the final design would require significant shielding.

The coils which were chosen for the design came mounted on a metallic base which is meant for shielding. The effectiveness of the shield was tested by comparing the voltage induced on the secondary when the coils were facing each other and the voltage induced when the coils were not facing each other. The measured SE of the metallic base was 10dB, which was expected for a copper sheet at the same frequency. In terms of power, only 1% of the incident power wave penetrates the shield.

The original research paper which served as the base for this project did not consider an EMI shield and so it appears that an SE of 10dB would be sufficient [1]. Additionally, a test device was placed above the coupled coils and no adverse effect was noted. It was determined that there would not be a need for any extra shielding.

3 Primary AC-DC Converter

Rectification of 120VAC from a standard wall outlet was required to provide the voltage supply for the wireless cellphone charging platform. Initial design consisted of rectification completed in two stages, AC-DC and DC-DC conversion. A full bridge diode rectifier was used to rectify the standard wall outlet voltage into a usable DC voltage. The second stage of rectification consisted of a Buck Converter to step down the rectified DC voltage into the desired 12VDC supply used for the wireless cellphone charging platform. A decision to purchase the primary AC-DC converter was made on the premise of safety, complexity, and cost.

3.1 Single Phase Bridge Rectifier

The circuit diagram below in Figure 3.1 depicts a single phase full wave diode bridge rectifier. Diodes D1 and D2 conduct during the positive half cycle of the AC voltage input while diodes D3 and D4 are off. During the negative half cycle of the AC voltage input, diodes D3 and D4 conduct while diodes D1 and D2 are off. The resulting waveform is equal to the positive half cycle of the input voltage waveform with twice the frequency as seen in Figure 3.2 below [4].

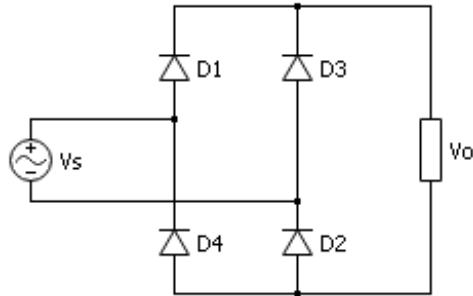


Figure 3.1: Full wave bridge rectifier schematic.

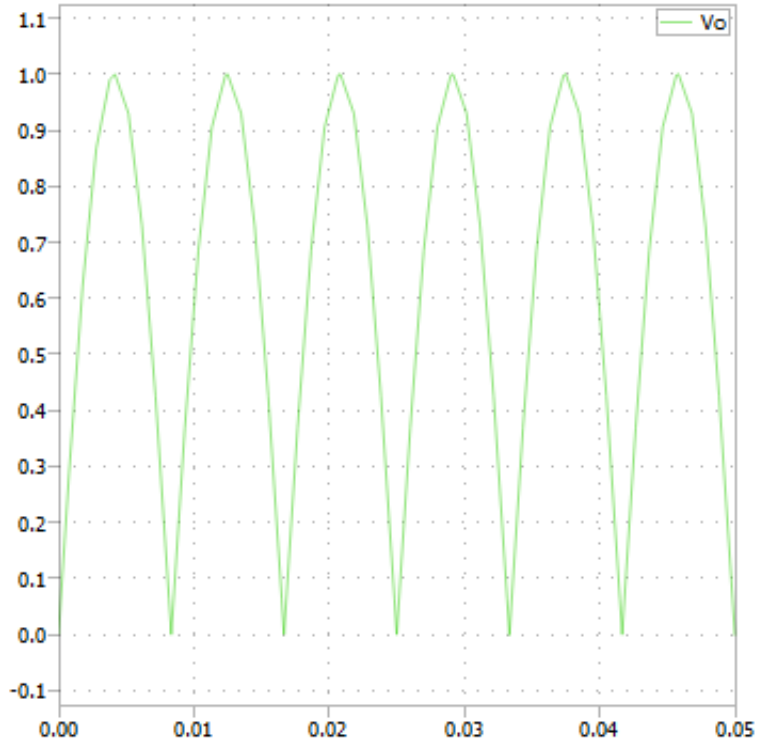


Figure 3.2: Full wave bridge rectifier waveform.

To create an almost pure DC waveform, a capacitive filter was placed in parallel with the output of the bridge rectifier. The capacitor was chosen such that its discharge was slow enough to maintain the output voltage at the peak value of the AC input. The output DC waveform can be further improved by adding a series smoothing inductor to the circuit. The circuit diagram for a bridge rectifier with a smoothing inductor and a capacitor filter can be seen in Figure 3.6 [4]. Design equations are provided in the following sections for determining the size of the capacitor and inductor added to the circuit to improve the output DC waveform.

3.1.1 Initial Design

The initial design of the full bridge diode rectifier was reached using Equations 3.1 and 3.2 [4].

$$L > \frac{R}{3\omega} \quad (3.1)$$

$$C = \frac{1}{\frac{\Delta V}{V}(2fR)} \quad (3.2)$$

The rectifier would not be directly connected to a resistive load and therefore the R value in the above equations was found from the voltage and power requirements at the output of the rectifier circuit. Equation 3.3 was used to determine the R value used to calculate L and C for the rectifier circuit.

$$R = \frac{V^2}{P} = \frac{\sqrt{2} * 120^2}{13.6} = 2,118\Omega \quad (3.3)$$

A 13.6W power requirement was determined from the target efficiency of 55% nominal specified in the design proposal. The expression $\Delta V/V$ defines the voltage ripple at the output which was chosen to be 1%. The capacitor and inductor sizes were then calculated to be $393\mu F$ and $1.87\mu H$ respectively. The calculated inductor was too large and resulted in a significant voltage drop creating large losses. For these reasons it was removed from the design. Additional justification for removing the smoothing inductor from the design will be presented in Section 3.4. The capacitor size was chosen as $470\mu F$ to slightly exceed the minimum calculated capacitance. The initial full bridge rectifier design is found below in Figure 3.3.

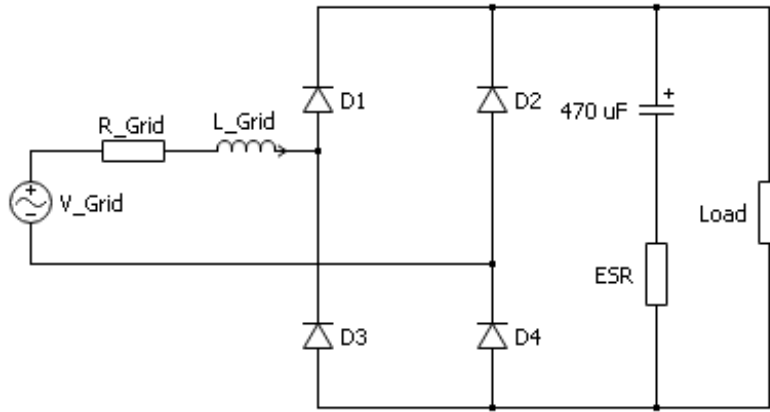


Figure 3.3: Full bridge rectifier initial design.

3.2 Buck Converter

Figure 3.4 below shows the circuit diagram of the Buck (Step-Down) Converter. A Buck Converter is a DC-DC converter that steps down the input voltage to a desired output voltage. When the switch is closed the diode becomes reverse biased and acts as an open circuit. When the switch is open, the diode becomes forward-biased and provides a path for the inductor current to flow. The operation of this circuit provides an output voltage that is equal to the input voltage multiplied by the duty cycle of the switch. Therefore, the switch duty cycle can control the DC output voltage to a value between 0 and V_s [4]. Detailed discussion of the Buck Converter circuit is not presented in this report and can be found in *Power Electronics* by Daniel W. Hart, Section 6.3 [4].

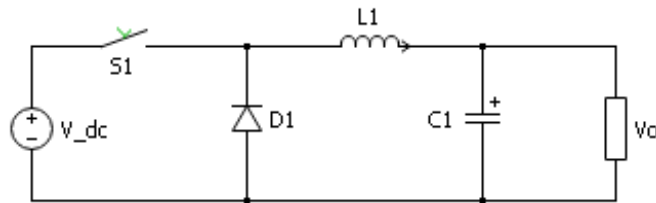


Figure 3.4: Buck converter schematic.

3.2.1 Initial Design

The output magnitude of the two stage AC-DC converter was chosen according to the following criteria: compatibility, voltage drop across the electromagnetic coils, and workability. A 12VDC output was determined as the starting point due to availability of parts with a 12V rating. The voltage required to charge a cell phone is 5VDC. A 12VDC output voltage is sufficiently high to ensure that the voltage drop across the inverter and

electromagnetic coils would not reduce the final load voltage to less than 5VDC. Another deciding factor of a 12VDC output voltage was the workability during building and testing. The component values for the buck converter were reached using the design equations below [4].

$$D = \frac{V_0}{V_i} = \frac{12}{\sqrt{2} * 120} = 0.0707 \quad (3.4)$$

$$C = \frac{1 - D}{\frac{\Delta V}{V} 8 L f^2} \quad (3.5)$$

$$L = \frac{(1 - D)R}{2f} \quad (3.6)$$

The duty cycle, D, of the switch in the buck converter circuit was found to be 7.07% as can be seen in Equation 3.4. The requirements of a 1% voltage ripple were maintained as in the rectifier design. The resistance value R was also calculated in the same way using Equation 3.3 with the corresponding output power requirements equal to 13.6W for reasons previously stated. To minimize component values, a switching frequency of 40kHz was chosen. Values of $59\mu F$ and $123\mu H$ were calculated from Equations 3.5 and 3.6 above. To meet the minimum calculated requirements for C and L, $68\mu F$ and $270\mu H$ were chosen respectively. The buck converter initial design is found below in Figure 3.5.

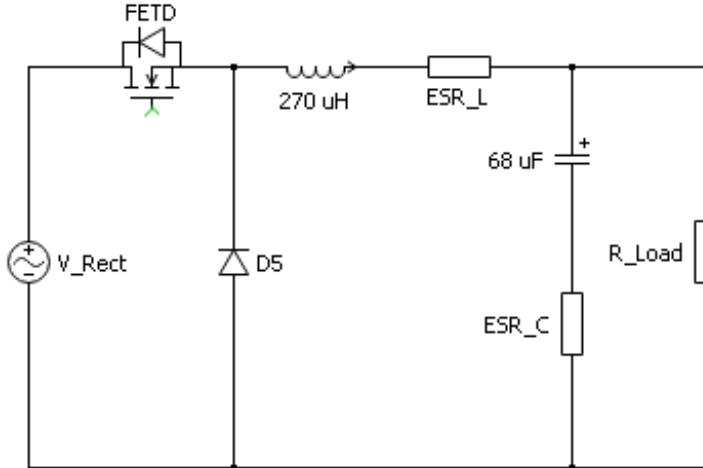


Figure 3.5: Buck converter initial design.

3.3 Reactive Power Compensation

Since the electromagnetic coils are an inductive load the AC-DC converter must be able to supply reactive power. Initial design assumed that the load would require an apparent power of $S_L = 80\text{VA}$. A shunt capacitor at the DC voltage supply output was designed to provide the reactive power required by the inductive load. Equations 3.7 and 3.8 below were used to determine the required capacitor size.

$$Q_{CSH} = \sqrt{S_L^2 - P_L^2} \quad (3.7)$$

$$C = \frac{1}{\omega \left(\frac{V^2}{Q_{CSH}} \right)} = 0.868\mu F \quad (3.8)$$

In order to provide a factor of safety, a $1.8\mu F$ capacitor was chosen which was double the minimum calculated capacitance.

3.4 Circuit Efficiency Considerations

An LC filtered output full bridge diode rectifier contains a series smoothing inductor, L1, as seen in Figure 3.6 below [4]. The inverter is supplying two planar surface coils which constitute a large inductive load. The reactive power requirements caused by this load created a large AC current through the series smoothing inductor. To meet the requirements of a high current rating, the inductor became physically large with undesirable equivalent series resistance (ESR). As previously mentioned, during simulations the large ESR caused significant losses across the inductor. Since the main design goal for the wireless cellphone charging platform was overall circuit efficiency, the smoothing series inductor was removed from the circuit. The inverter does not require a perfect DC voltage and a small ripple will not affect its function. Therefore, removing the smoothing inductor was justified.

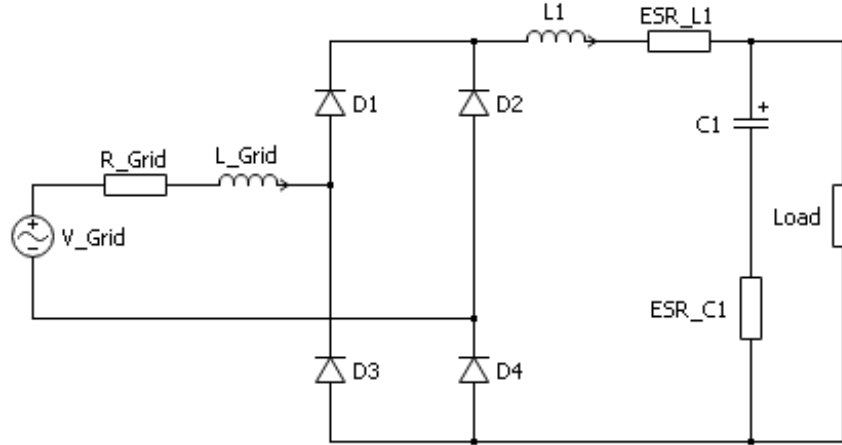


Figure 3.6: Full bridge rectifier with smoothing inductor.

Another design method considered was to step down 120VAC from the standard wall outlet with the use of a transformer. The issue with designing the rectifier in this way was the efficiency of the transformer. The use of a transformer would add another stage of inefficiency to the rectifier circuit. The power requirements to charge a cellphone are small, 7.5W at 5V, and any component that introduces a loss would have a large impact on the overall circuit efficiency. For this reason, the choice to move forward without an initial step down transformer was made.

3.5 Simulation and Results

Simulation results of the circuits in Figures 3.3 and 3.5 are shown in Figure 3.7. The simulations were performed without the shunt capacitor and with the above circuits connected in cascade to form a two stage AC-DC converter connected to a resistive load.

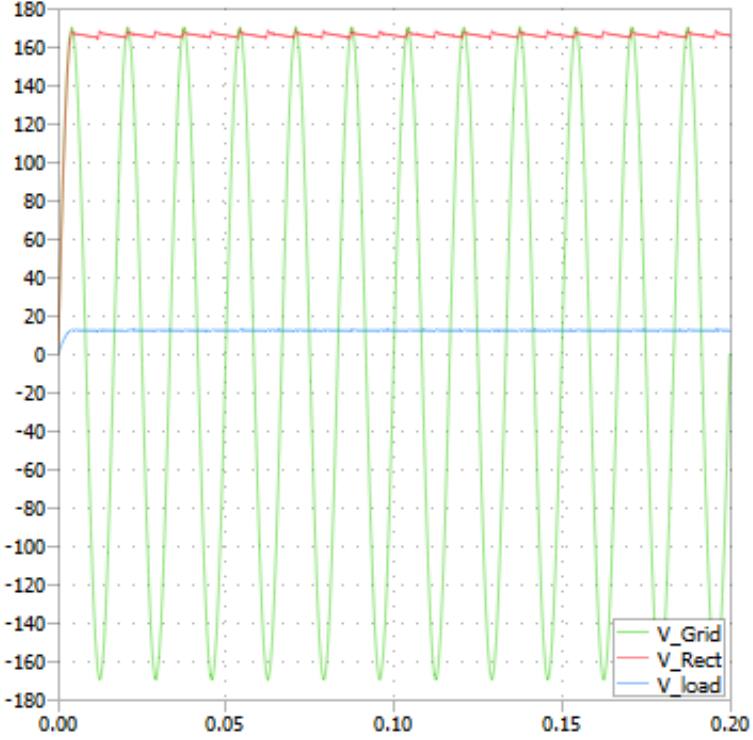
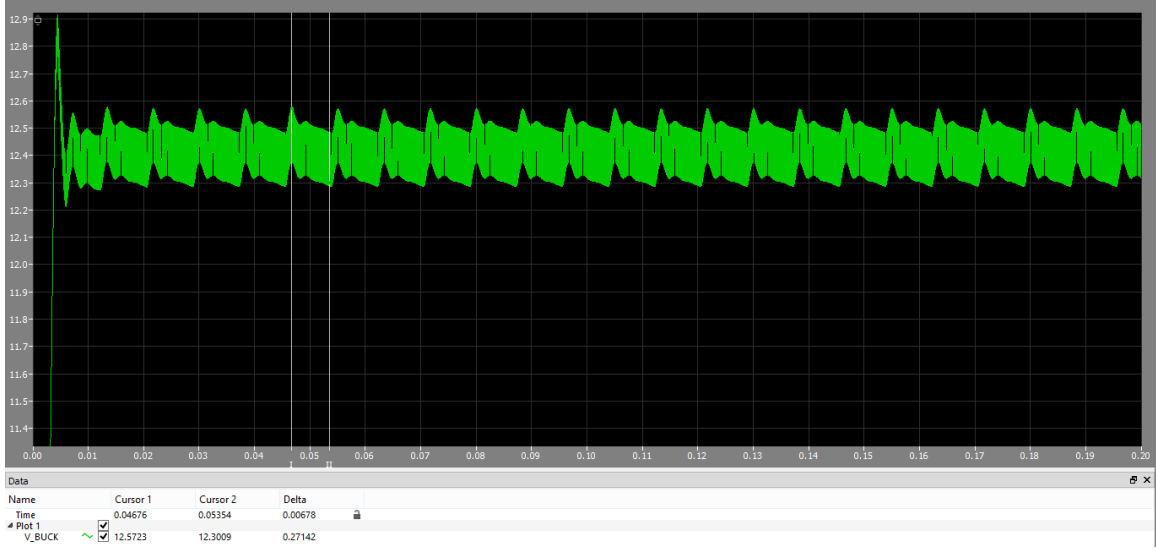
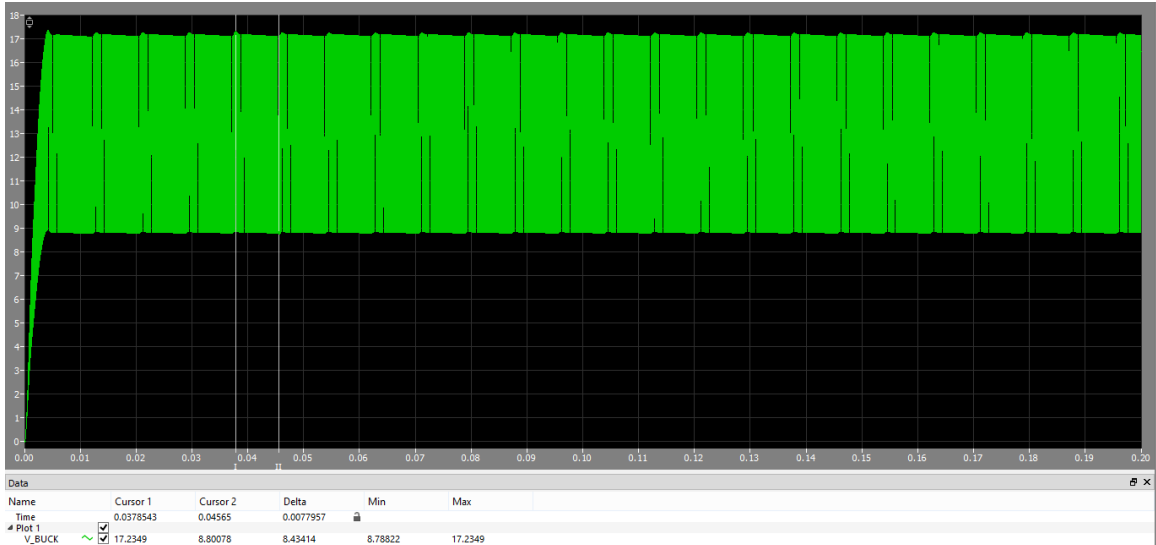


Figure 3.7: Two stage AC-DC converter voltage waveforms.

As can be seen from Figure 3.7, the output voltage had a Root Mean Square (RMS) value of 12 volts, therefore achieving the 12VDC set out in the initial design. The duty cycle was tuned to 0.0755 to produce a 12VDC output. The blue waveform shows the output voltage of the two stage AC-DC converter. The output had a small voltage ripple which was desired in the initial design. Since this simulation was performed with a resistive load, this voltage ripple will only increase when connected to the inverter and coils. As previously mentioned, a reactive power compensating capacitor was connected in parallel at the output of the AC-DC converter. The capacitor was chosen to be $330\mu\text{F}$ to meet the ripple current requirements through the capacitor observed during preliminary simulations. The choice of a larger capacitor only improved the design and added an additional factor of safety. The two stage AC-DC converter was then simulated with the complete project circuit, as shown Appendix B, to investigate the performance of the shunt capacitor. Figure 3.8 (a) and (b) below show the output of the two stage AC-DC converter with and without reactive power compensation, respectively.



(a)



(b)

Figure 3.8: Two stage AC-DC converter output. (a) With shunt capacitor. (b) Without shunt capacitor.

It is obvious from the figures above that the shunt capacitor drastically improved the design. With the shunt capacitor connected at the output of the AC-DC converter, the voltage ripple was significantly reduced to a value of 2.26%. This voltage ripple is slightly higher than the initial target of 1%, but is acceptable as the DC supply to the inverter circuit.

3.5.1 Physical Implementation

Consideration of safety, complexity, and cost led to the decision to purchase the primary AC-DC converter. This decision was best for the project as the purchased circuit contained a known circuit efficiency, output voltage ripple, output power and maximum inrush current. The purchased AC-DC converter was chosen to meet all important design criteria at a fraction of the cost to build the circuit. In the paragraphs below, justification is provided for the decision to purchase the AC-DC converter.

If the AC-DC converter was built, the implementation would require working with 120VAC. Limited testing equipment was available for this high of a voltage rating and without experience, working at this voltage can be dangerous and even fatal. Purchasing a power supply eliminates the risks and safety hazards associated with 120VAC all together.

Building a functional AC-DC converter adds further complexity to the overall project. The second stage of the AC-DC converter functions to step down the voltage to the required 12VDC. The metal-oxide semiconductor field-effect transistor (MOSFET) switch shown in Figure 3.5 requires control from the Arduino UNO. The Arduino UNO would need to provide a pulse to the gate pin of the MOSFET to turn on and off the switch. This additional control would put unnecessary strain on the Arduino UNO and would likely result in further circuitry to amplify the gate pulse to an appropriate level of current. The reactive power requirements due to the inductive load caused significant amounts of AC current in the AC-DC converter circuit as determined during simulations. For this reason, the component values required large power ratings which made purchasing the components difficult. The availability was limited and the physical size of the components was too large with significant ESR values. In turn, the efficiency would be reduced if these components would be used. Another addition to the complexity of the project is the unknown circuit efficiency of a built AC-DC converter. With a purchased AC-DC converter, the efficiency is specified and can be chosen to be minimized.

As previously mentioned, cost was a significant factor in making the decision to purchase the AC-DC converter. The large voltage and current requirements increased the price of each component and the overall circuit became comparable to, or more expensive than a purchased AC-DC converter. The fact that buying a pre-built AC-DC converter which met the project requirements had the same cost as building one from the ground up made the decision to purchase one clear.

The decision to purchase the primary AC-DC converter was based on the premise of safety, complexity and cost as described in the above sections. When determining which converter to buy, original design criteria such as efficiency, output voltage ripple, and output power were considered. An Inventus Power IPD20 SERIES CLASS I 20W ITE Desktop Power Supply was chosen with the technical specifications listed in Table 3.1 [5].

Table 3.1: AC-DC power supply technical specifications [5].

Efficiency	88.40%
Voltage Ripple	< 1% pk-pk
Output Power	20W
Over Voltage	112-135%
Over Current	108-180%
No Load Power	< 0.1W
Inrush Current	60A

Another consideration when purchasing the power supply was protection. This power supply would be used during testing of the inverter circuit and may be exposed to short circuiting, overvoltage or overcurrent. The chosen power supply contains short circuit protection, overvoltage protection, and overcurrent protection [5]. This way, the appropriate protection is integrated into the power supply to prevent damage during building and testing of the inverter circuit. Another benefit of this specific power supply is the no load power consumption. There will be significant time when the wireless cellphone charging platform is plugged in but is not charging a cellphone. This specific power supply has less than a 0.1W no load power consumption which is desirable for this application [5]. During operation of a wireless cell phone charging platform, the cell-phone will be continuously placed on the charging pad going from no load to full load each time. For this reason, the inrush current requirements were investigated during simulations and compared to the purchased AC-DC converter. Figure 3.9 shows the inrush current requirements realized during simulations.

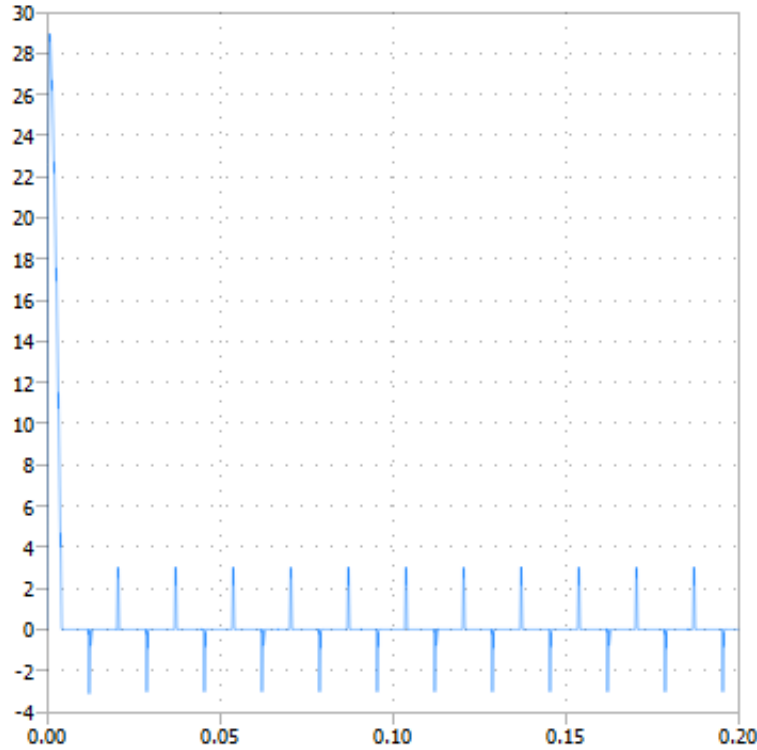


Figure 3.9: AC-DC converter inrush current requirements.

The inrush current requirements above are shown to be approximately 30A. The chosen power supply has a maximum inrush current rating of 60A which allows a safety factor of 2 [5]. For the many reasons stated in this section, the choice to purchase an AC-DC power supply was justified and provided a better result for the project.

3.5.2 Testing & Results

Isolated testing of the AC-DC converter consisted of connecting the power supply to a resistive load to determine that the voltage output was in fact 12VDC. The test was a simple check to ensure correct functioning before termination to the inverter circuit.

4 Arduino

The Arduino served two main purposes. First, to detect the presence of a cell phone in proximity to the charging platform and second, to control switching of the inverter supplying power to the primary side coils.

4.1 General Overview

To indicate whether the charging platform was in hibernation or currently charging, there was a single tri-color light emitting diode (LED) protruding from the charging platform. The tri-color LED would flash red to indicate that the platform was in hibernation. During this time the RFID transmitter would be actively searching for any cellphones within proximity. Once a cellphone was detected by the RFID transmitter, the tri-color LED would be solid blue. The inverter would be activated, power would then be supplied to the primary coil, and charging would begin. During this time, the RFID transmitter would intermittently search to verify the presence of the cellphone. Inability to detect the cellphone would result in a return to the hibernation state. The flow chart of Figure 4.1 summarizes the Arduino's control process.

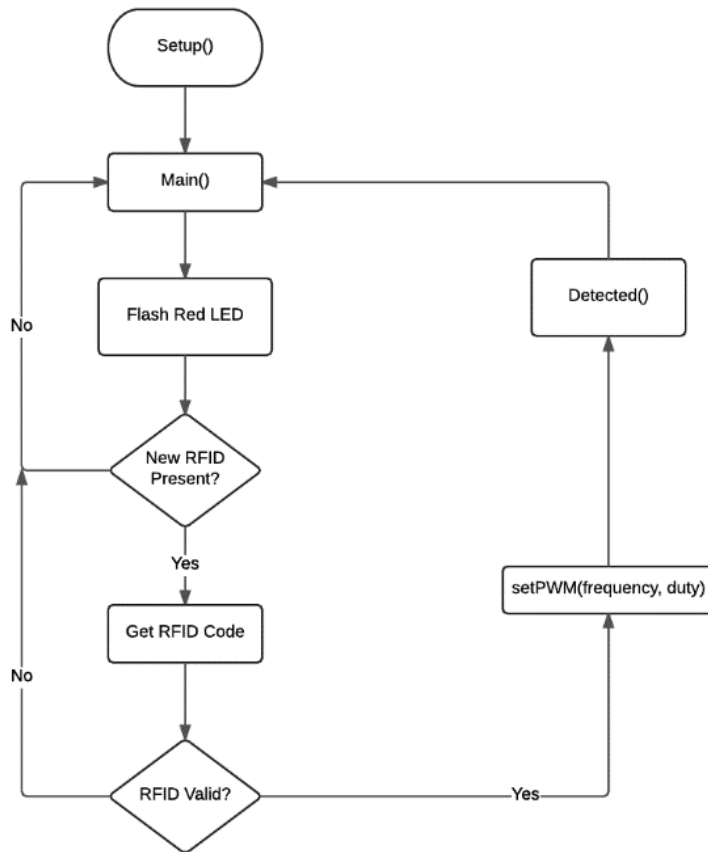


Figure 4.1: Arduino control process.

4.2 Cell Phone Detection Module

The ability to detect the presence of a cell phone on the charging platform was necessary as it offered the ability to minimize power consumption. When a cell phone was not within range of the charging platform, the inverter would enter a state of hibernation to reduce power consumption.

4.2.1 Design Considerations

Early considerations with respect to the concept of cellphone recognition focused on the use of a photoresistor. This mode of operation would detect the cellphone via the absence of light. This idea was quickly rejected for its inability to provide any distinction between a target device and any other object obstructing the sensor. An alternative choice was the use of a MFRC522 RFID chip. This RFID sensing module is a passive device which serves the purpose of activating the primary inverter circuit when the device is within range of the RFID reader. A number of tests through materials with a permittivity of $\mu=1$ were conducted, indicating that a maximum effective detectable range of 2cm would be consistently possible. Although this range was relatively short when compared to some of the passive, Ultra High Frequency tags currently on the market, which can be read from distances exceeding 20ft³, this would be unnecessary as the charging platform cannot effectively transfer power across such a distance. Since the RFID tag was written with a unique identification code, it provided a method of detection protocol to eliminate the possibility of activating the inverter when non-chargeable devices were placed on the charging platform.

The primary concern pertaining to the usage of an RFID sensor was the possibility of electromagnetic interference occurring between the charging coils and the RFID transmitter. Dr. Ahmed Byagowi was confident that if the operating frequency of the RFID tag and the charging coils were different then there would not be an issue. With the operating frequency of the charging coils in the range of kHz and the RFID tag having an operating frequency of 13.56MHz [6], the use of the selected RFID tag was accepted. As an additional measure, the RFID transmitter-receiver pair and the charging coils were placed separately within the circuit. This placement is apparent in the case design of Figure 7.1.

³<https://www.rfidjournal.com/faq/show?69>

4.2.2 Implementation

Figure 4.2 depicts the physical layout of the RFID-Arduino connections. The code developed is provided in Appendix C, and utilizes an Arduino library obtained from Github.com [7].

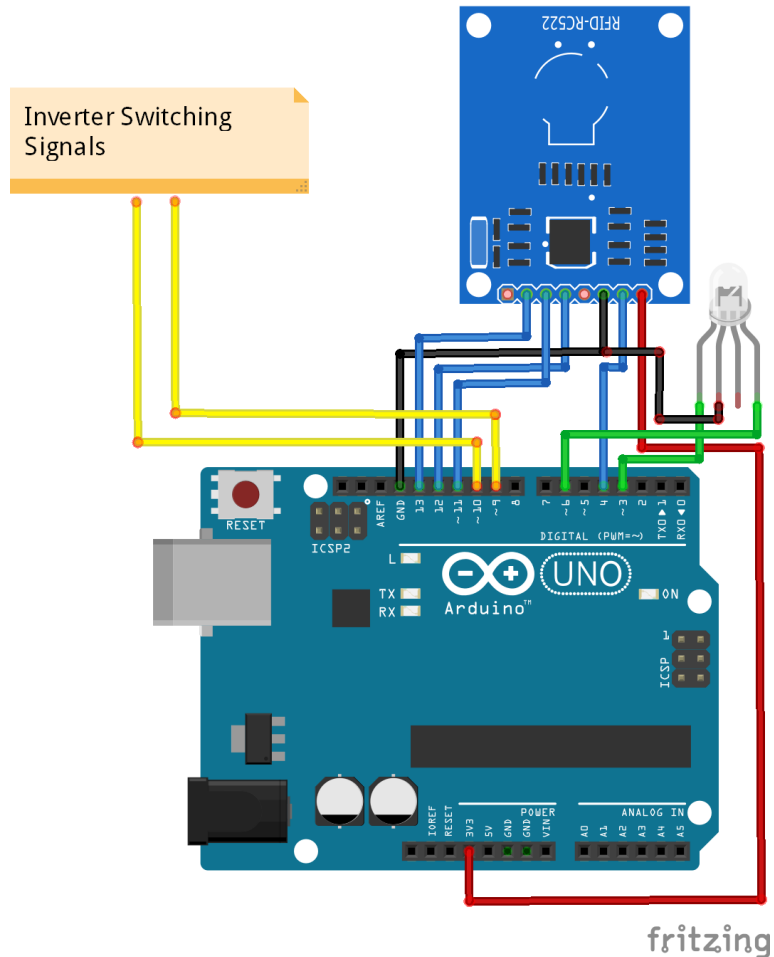


Figure 4.2: Control circuit wiring diagram.

4.3 Inverter Signal Generation

Inverter control was the most significant task performed by the Arduino in this design. It must accurately supply and maintain signals in excess of 100kHz to the four inverter MOSFET switches, while maintaining the ability to adjust the switching frequency. Accuracy was crucial as mistimed signal switching could result in contention and short circuits harmful to the electronics.

4.3.1 Design Considerations

Initially the generation of a signal to supply the primary coils was to be accomplished using four digital pins of the Arduino. Each pin would be set to 0VDC or 5VDC with the required delays included to generate an AC square waveform with the required frequency to control inverter switching. This approach appeared feasible since the Arduino's clock speed is 16MHz [8]. It became obvious that this approach was not feasible as the list of responsibilities which the Arduino would have to accomplish was growing. Additionally, the Arduino would be incapable of supplying the high current draw required by the coils. Alternative approaches included the use of a motor driver or a master-slave arrangement, in which the slave would be responsible for generating the switching signals. Motor drivers with high current and frequency capabilities were not readily available. The Arduino's ability to perform pulse width modulation (PWM) was determined to be the most effective technique.

The Arduino's built in PWM pins have fixed frequencies of 490Hz with the exception of pins 5 and 6 having a frequency of 980Hz ⁴. This limitation made use of the pre-programmed PWM function not feasible. Further research provided details regarding the modification of the Arduino's PWM timers. Through modification of the ATmega328p timers directly, the Arduino PWM outputs could be increased to the needs of the inverter ⁴. However, modification of Timer0, which controls delay functions, undesirably changes all time keeping functions of the Arduino ⁴.

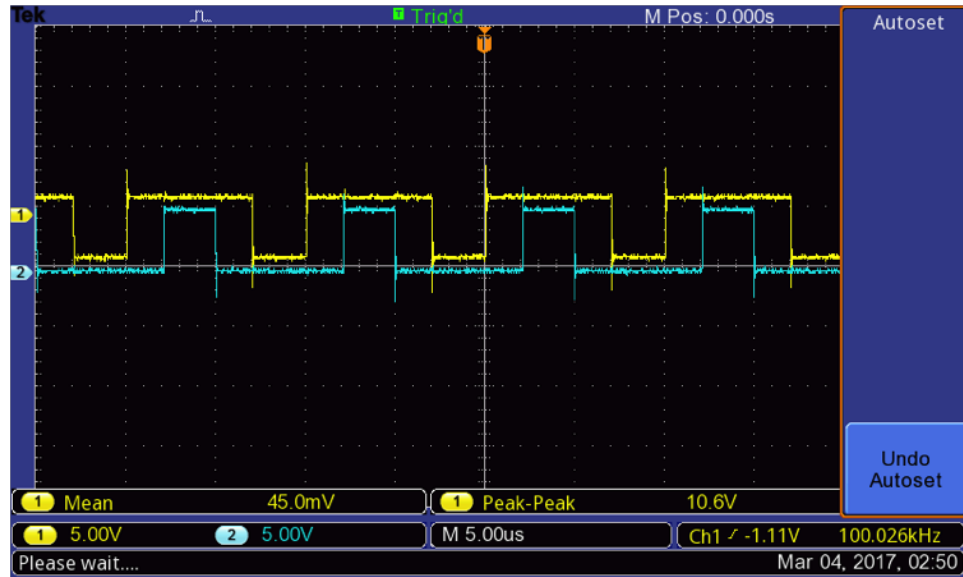
A PWM library containing functions to adjust the frequency as high as 2MHz was found on the Arduino Forum [9]. This library included functions which would preserve the state of Timer0 in order to protect the Arduino time keeping functions. Since each PWM capable pin shares the internal timers with other PWM pins, frequency adjustment of one PWM pin may adversely affect the PWM abilities of other pins. As a result, specifying the frequency of a PWM pin would eliminate the functionality of other PWM pins.

4.3.2 Implementation

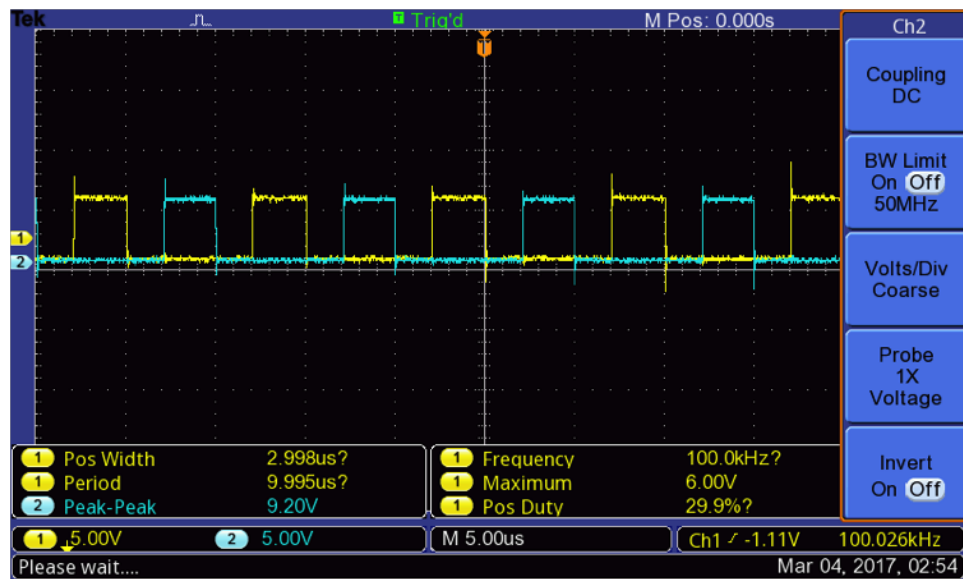
During testing it was determined that operation above 100kHz would limit the number of functional PWM pins to two, as explained in the previous section. Initially this posed a problem as four pins would be required to control the four MOSFETs of the inverter. Use of gate drivers and inverting circuits were implemented, as described in Section 5.4.3, as a solution to the problem. Since the PWM pins operation are dependant on mutual timers their outputs generate a predictable signal with respect to one another. By making

⁴<https://www.arduino.cc/en/Tutorial/SecretsOfArduinoPWM>

certain that the duty cycle of each signal differs by a suitable margin, simply inverting one of the signals would produce a switching control with the dead time required to prevent contention. This concept is illustrated in Figure 4.3.



(a)



(b)

Figure 4.3: Gate driver signals. (a) Non-inverted signal. (b) Inverted signal.

5 Inverter

The conversion of DC voltage to AC voltage is achieved by a converter known as an inverter. The inverter stage was required to drive significant amounts of current through the planar coil in either direction. An H-Bridge inverter is normally used to supply a bi-directional DC motor for its ability to drive current, and therefore the motor, in either direction. The planar coil is an inductive load similar to a motor and the bi-directional, or alternating current is required to create the magnetic field. Therefore, the H-Bridge topography was selected to drive the primary side planar coil with AC voltage. The H-Bridge switches were selected to be power MOSFETs for their high switching capabilities and low gate power requirements. Gate drivers were used to drive the switches for their power delivery and isolation capabilities.

5.1 Design Considerations

The magnetic field generated by the planar coils is directly proportional to the frequency of the voltage applied. The operating frequency, though it changed multiple times throughout the project, was in the 30-150kHz range. Therefore, the capability of the switch to turn on and off quickly was a major consideration. Another consideration was the amount of current that would pass through the switches into the coil, which was approximately 7A. The larger the resistance of the switch while conducting, the more power losses are incurred. At high current, these losses become significant and since a major design goal of the project as whole was efficiency, reducing losses in the switches was important. Therefore, the drain-source resistance (R_{ds}) value of the switch was to be as low as possible. The MOSFET was selected for its fast switching ($>200\text{kHz}$) and power delivery capabilities. Additionally, MOSFETs require negligible gate current compared to insulated-gate bipolar transistors thus the driving requirements are less power intensive.

A major design consideration throughout the project was how the gates of the switches would be driven. The two factors of most concern were the voltage level required to drive the switch as well as isolating the controller from the rest of the circuit to avoid damage. The controller outputs logic-level voltage (5V). However, since conduction is determined by the voltage difference between gate and source (V_{GS}), as the source voltage approaches the gate voltage conduction begins to slow/stop. As the load voltage was to be 10-12V, the switch would not conduct to supply the load with this voltage using a 5V gate signal.

5.2 MOSFETS

An important design goal was the efficiency of the overall device. As such, it was especially important to consider the losses of the components used in the inverter as the current values were highest in this portion of the device. Therefore, the model and operating point of the switches had to be carefully considered.

The MOSFET is a three terminal semiconductor device with a wide range of applications in amplification and logic circuits. The physical structure consists of a gate, source and drain semiconductor region. The regions are “doped” differently creating an environment for the conduction of current to occur. The regions have metallic electrodes attached to them to allow flow of current outside of the device [10].

Doping refers to small amounts of impurities which are introduced to the silicon to provide a higher or lower concentration of electrons, or charge carriers. N-type doping is when substances with more valence electrons than silicon are introduced. These donor atoms use 4 of their valence electrons to bond with surrounding silicon and the other is left orbiting the doping site. P-type doping is when substances with less valence electrons than silicon are introduced. These acceptor atoms use 3 of their valence electrons to bond with the surrounding silicon atoms. The last unformed bond, or hole, can be filled by free electrons. [11].

N-type MOSFET technology was used for the inverter switches. The source and drain regions are smaller and are n-type material. The body, to which the gate electrode is attached, is a larger p-type material bridging the source and drain together. When no voltage is applied to the gate electrode, the body is a very high resistance ($\sim 10^{12}\Omega$) region that allows virtually no current through when there is a voltage applied across the drain and the source (V_{DS}). When a positive voltage is applied to the gate, creating a positive voltage difference between gate and source, a channel for current flow opens up. This channel is created by repelling the holes to the bottom of the region as well as attracting the free electrons to the top of the region. This newly induced region is effectively n-type like the source and drain regions. Now when a small V_{DS} is applied, this voltage causes mobile electrons to travel towards the drain through the low resistance channel ($\sim 10^{-2}\Omega$). The V_{GS} required for sufficient conduction is known as the threshold voltage. Up to a point, as V_{GS} increases, the channel resistance lowers and the losses incurred during conduction decrease. The gate electrode - body junction appears as a capacitive load to the source providing the gate charge [10].

$$P_{loss} = \frac{V_{DS}^2}{R_{DS}} \quad (5.1)$$

Conduction losses in the channel come in the form of heat in the body and are quantified by Equation 5.1. When the MOSFET is not conducting optimally, R_{DS} increases and higher losses incur. To achieve the lowest R_{DS} as possible and thus the maximum power delivery to the load, V_{GS} should be as high as required by the desired i_D . Additionally, the transition time between on/off states should be quick as possible.

5.3 H-Bridge

The H-Bridge topography is named so because of its “H” shape formed by four switches and the load. The two conducting paths for current are formed by pairs of “top” switches and “bottom” switches through the load. Control signals to the gates of the pairs are complemented so that only one path is conducting at a time. In the case of an inductive load, dead time can be added to allow for the continuous conduction of current through a path to dissipate [4]. The two paths are depicted in Figures 5.1 (a) and (b) below.

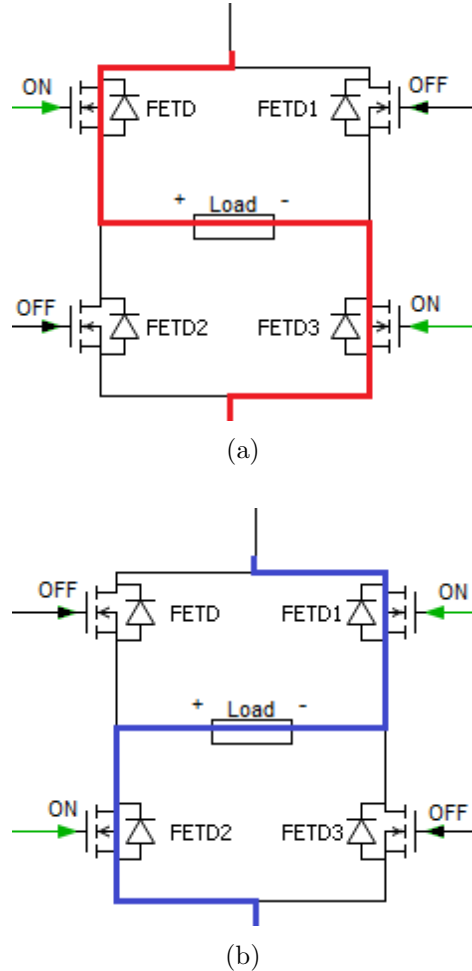


Figure 5.1: Alternating current paths for the H-Bridge inverter. (a) Path 1. (b) Path 2.

The simulated circuit (Figure 5.2) included the 12VDC source, appropriate gate voltages to each switch (12/24V), the dead time between each signal and the series capacitor plus planar coil load. Additionally, the secondary planar coil plus load (3.3Ω to simulate input resistance of the phone) was coupled to the primary coil. A $600\mu\text{F}$ capacitor was put in parallel with the source to provide the reactive power required by the load. This reactive compensation prevented voltage drop at the source during periods of conduction.

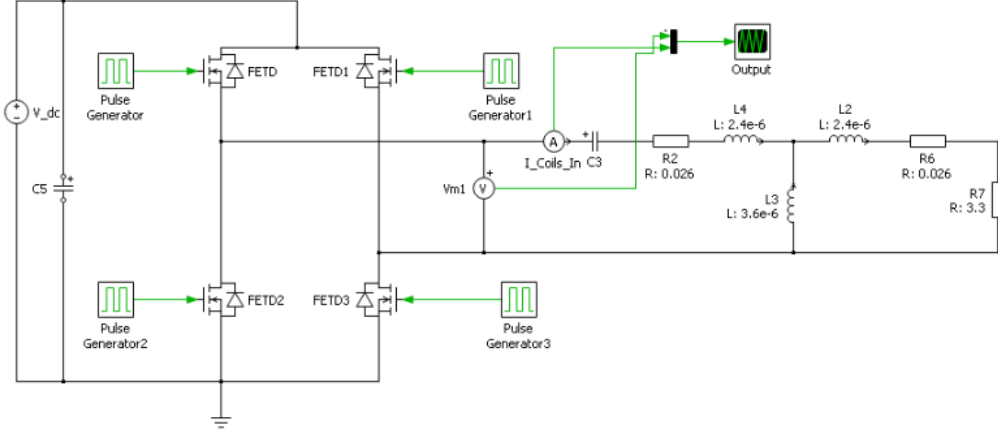


Figure 5.2: The inverter circuit.

5.3.1 Initial Simulation

The pulse generators provided voltage for 30% of a 100kHz signal which allowed for 20% dead time between each path conduction. The initial simulation was completed assuming ideal switches (instant conduction, low threshold voltage and no losses). It was quickly apparent that physical properties of the switch and gate driving voltages should be considered to achieve more meaningful results. After specifying physical MOSFETS, a conduction resistance of 0.075Ω was added to the switch models. Additionally, “Pulse Generator” and “Pulse Generator1” had their output voltages increased to 24V as per the V_{GS} requirements of the top switches. The resulting current and voltage waveforms are shown in Figure 5.3 below.

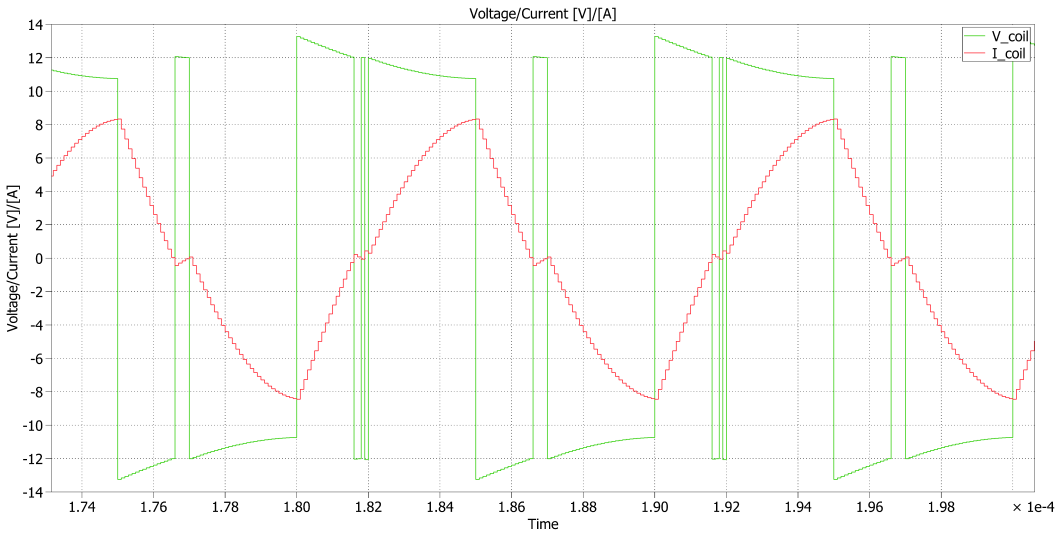


Figure 5.3: The simulated inverter output into the primary planar surface coil.

Even with the physical parameters added it was expected that the simulated waveform would not have properties that would appear in the final build. The instantaneous rise and fall of 24V and the resonating voltage during dead time were expected to be damped in practice.

5.3.2 Second Simulation

A second simulation was performed later using a lower frequency of 32kHz. This operating point was simulated in case the supporting electronics (gate drivers, Arduino and load) limited the switching speed of the inverter in real life. The frequency was chosen on the lower side of the resonance peak ($\sim 72\text{kHz}$). The main takeaway was to be the efficiency of the inverter with the same load parameters as the initial simulation (3.3Ω at 0.6 coil coupling). The DC current out of the source was 620mA and the RMS current into the load was 1.2A. This translated into 7.44W and 4.75W respectively for a calculated efficiency of 63%. This efficiency value includes the coil losses.

5.3.3 Third Simulation

A third simulation was performed at a higher frequency of 160kHz. Once a low frequency operating point was established for the real circuit, an operating point on the high side of the resonance peak was to be explored to possibly increase efficiency. The DC current out of the source was 705mA and the RMS current into the load was 1.52A. This translated into 8.46W and 7.62W respectively for a calculated efficiency of 90%.

5.4 Driving The H-Bridge

The physical implications of driving the H-Bridge were not realized completely in the initial simulation. Several supporting electronics were required to provide control to the switches. These supporting electronics consisted of a signal inverting circuit (NOT circuit) and gate driving circuit. For the gate driving circuit, pulse transformers and gate driver ICs were considered. These supporting electronics created an additional power burden on the source, which affected the overall efficiency.

5.4.1 Pulse Transformers

Pulse transformers were one of the methods considered for driving the inverter switches. Pulse transformers work to reduce voltage droop and distortion of a pulse under a load⁵. They operate with a magnetizing current that does not cross the zero point. The initial idea was to use 5/12V pulse transformers to transform the pulse train from the Arduino to a pulse train of higher magnitude which would drive the gates of the switches. The idea was abandoned quickly as it did not meet a number of the requirements. Firstly, the initial rise of the 5V pulse could not create a pulse for the entire duration on the secondary side. The maximum pulse length was approximately $1\mu s$ which is much lower than the $3-10\mu s$ that was being considered. Secondly, in the case of a switch failure drawing current from the gate, the Arduino would not be electrically isolated. Current drawn on the secondary side will draw current from the primary side until magnetic saturation. Lastly, when considering the need for a higher than 12V gate signal on the top switches, a single pulse transformer would not be able to achieve this. These considerations introduced the need for gate driver integrated circuits.

5.4.2 Gate Drivers

Gate drivers were used to amplify the low power control signal from the Arduino into a high voltage signal. This signal was used to provide power to the gates of the inverter MOSFETs. Since MOSFET gates are voltage driven, the driver acted to supply charge and remove charge to the gate electrode at turn on time and turn off time respectively. A simple functional diagram of a gate driver is shown below in Figure 5.4. When the input signal is high, a switch provides current to charge the gate of the MOSFET. When the input signal is low, a switch drains the charge from the gate of the MOSFET to ground [12].

⁵<http://www.butlerwinding.com/pulse-transformer-operating-principles/>

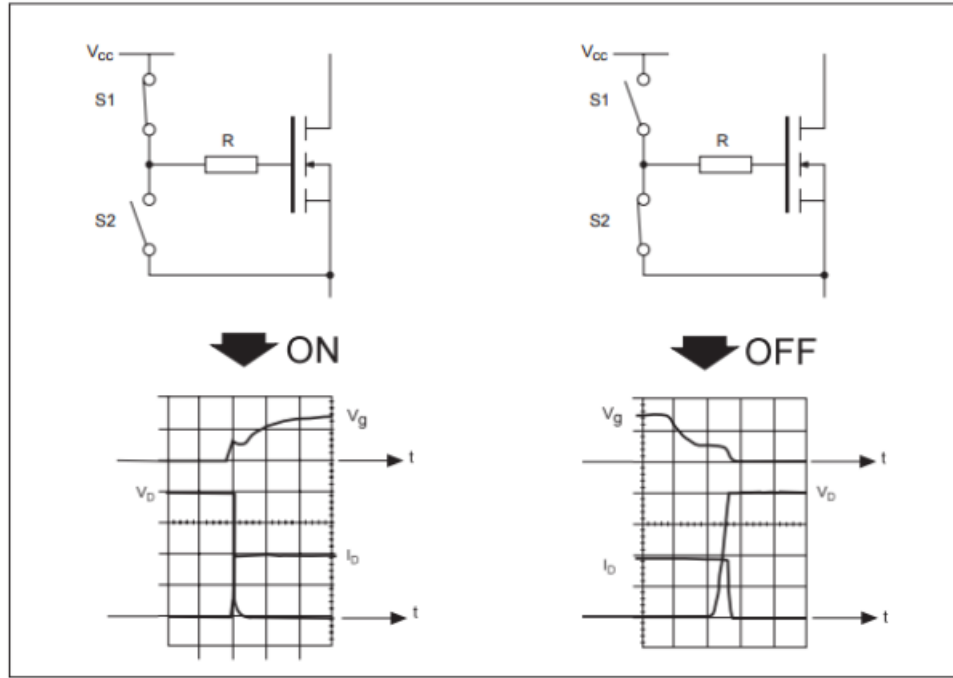


Figure 5.4: The gate driver output [12].

There are various methods of input amplification which is further discussed in Section 5.5.2. The resistor between the output and the gate was used to limit current output in the event of a supply or switch failure.

5.4.3 NOT Circuit

In order to accomplish the control signal generation outlined in 4.3, an inverting device, not to be confused with the DC-AC inverter, was required. The main considerations were the current driving ability, speed and signal integrity. The control diodes of the gate drivers each required approximately 10mA of current which could be easily provided by the 5V pin of the Arduino. Since the signal on the 5V pin was directly rectified from the source and not connected to the microcontroller chip, it could provide $\sim 900\text{mA}$ without damaging the chip. A single lower power, n-channel MOSFET (2N7000) was used with a current limiting resistor Figure 5.5. To ensure the inverted signal was as close to the non-inverted signal as possible in terms of edge time, a voltage supporting capacitor was placed between the 5V pin and ground.

When the pulse train was high, the switch turned on and the current flowed through the 100Ω resistor through the switch to ground. The voltage at the drain of the switch which is seen by the gate drivers was effectively 0V (aside from a negligible

V_{DS}). When the pulse train was low, the switch turned off and voltage was divided between the 100Ω resistor, 330Ω resistors and gate driver diodes. The gate driver diodes required approximately 1.1V to turn on, and as such the remaining voltage was divided among the resistors. Through trial and error, an appropriate resistor ratio that would provide enough current, while still limiting losses during switch conduction (off time) was selected. The final circuit was adequate enough to provide a control signal that would allow the pairs of gate drivers to perform identically.

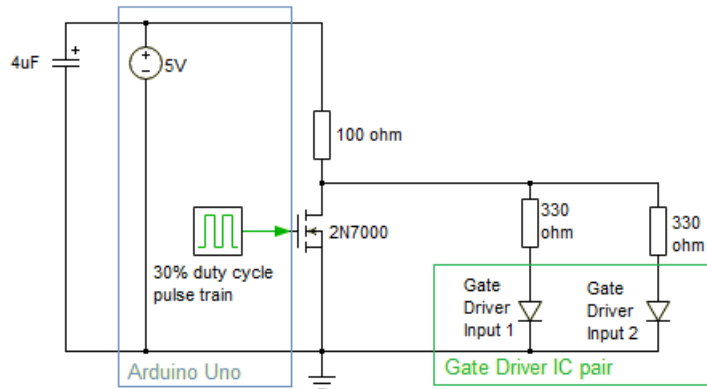


Figure 5.5: The NOT circuit.

5.5 Building the Inverter

The inverter was built on perforated project board using through-hole mounted parts. Assuming a maximum rated current of 10A, 12 guage wire was selected for the high current paths between the switches and the load. The gate driver ICs selected required some supporting resistors and bypass capacitors. Additionally, a DC-DC converter was included to increase the supply voltage to the top switch drivers.

5.5.1 H-Bridge MOSFET and Wire Selection

The actual MOSFET switches used for the inverter, along with the previously mentioned considerations, were selected on mounting and availability. As such, the IRFP250NPBF power MOSFET was selected. The relevant features of this switch are listed in Table 5.1 below.

Table 5.1: MOSFET parameters [13].

Drain Current Rating (I_D)	30A
Threshold / Optimal Operating V_{GS}	2.0 / $\sim 10V$
On Resistance at $V_{GS} = 10V$	0.075Ω
Transition Times	< 100ns dependant on load inductance
Mounting	Through-hole

The through-hole mounting of the switch was a necessary feature in order to perform early testing on a breadboard. The decision to build the circuit on perforated project board instead of a PCB allowed the use of the switches in the final build. This decision was also based on PCB lead time and the group's lack of PCB design experience. The H-Bridge circuit was fairly simple in its number of parts and low number of connections, but also required high current levels through some paths. As the current through the H-Bridge was to be 6-8A depending on operating frequency, concerns over PCB trace sizes arose. It was thought best to use perforated board and high gauge wire for the load paths. 12 gauge wire was selected for all path through the bridge based on the American Wire Gauge guide which indicated a rating of 10A. Although the resulting current to the load is high frequency and alternating, the current through a switch pair path is direct. As such, skin effect was not considered in the sizing of the wire.

5.5.2 Gate Driver Selection

The HCLP-3180 Gate Drive Optocoupler was selected to perform the gate driving of the H-Bridge. This IC was selected primarily for the fact it was the fastest switching gate driver that could be through-hole mounted. The optocoupler works by applying current to an LED which emits light, activating the output circuit. This also provides electrical isolation between input and output. The relevant technical specifications of this gate driver are listed in Table 5.2 below.

Table 5.2: Gate driver technical specifications [14].

Supply Voltage Limit (V_{cc})	25V
Threshold / Optimal Operating V_{GS}	2.0 / $\sim 10V$
On Current	8mA
Max Forward Voltage (Control Input)	1.8V
Transition Times	25ns
Mounting	Through-hole

The gate drivers required $0.1\mu F$ bypass capacitors at their supply rails to protect them from source transients. A resistor between the 5V pulse train control voltage and the input was required to ensure less than 1.8V was dropped across the diode. Lastly a 15Ω resistor was placed between the output and the gate to limit the initial surge of current required to charge the gate.

To calculate the input resistor value, a worst case 1.8V drop across the diode and 8mA turn on current were assumed. The resistor values for the non-inverting and inverting inputs were then calculated as in the equations below.

$$\frac{5V - 1.8V}{8mA} = 400\Omega \quad (5.2)$$

$$\frac{5V - 1.8V - (150\Omega * 8mA)}{8mA} = 250\Omega \quad (5.3)$$

The physical values used were 390Ω and 330Ω respectively. They provided adequate current and protection for the LEDs; this was confirmed by the proper operation of the gate drivers.

5.5.3 DC-DC Converter

To provide a peak voltage of 12V at the source pins of the inverter switches, the gate voltage supplied to the top switches was required to be significantly larger than 12V. This was to allow consistent conduction of the MOSFETs regardless of load voltage. With only 12V supplied to the gate drivers, the ability of the top switches to conduct suffered greatly as the load voltage approached 12V (V_{GS} approaching 0V). The reduced conductivity resulted in a voltage drop of up to 6V across the switches, and subsequently generated an excessive amount of heat, and a greatly reduced voltage at the load. A DC-DC converter was used to boost the 12V supply to 24V at the gate drivers of the top switches. This solution resulted in a V_{GS} of 12V for a load voltage of 12V. This allowed adequate conduction through the top switches during the entire duration that current flowed through each path. This was the final step in producing a waveform that would provide enough power to the secondary load.

5.6 Operation Results of Inverter - No Coupling

The main objective of testing the inverter without the secondary load was to establish that it could provide the coil with a $24V_{pp}$ waveform similar to the simulated one. Figures 5.6 and 5.6 below are the output voltage of the inverter at 30kHz and 160kHz, 30% duty cycle, which were figured to be the limits of operation points that would be tested.



Figure 5.6: Inverter output waveform at 30kHz.



Figure 5.7: Inverter output waveform at 160kHz.

These were deemed acceptable output voltage waveforms for the coil to produce an alternating magnetic field. The operation point and efficiency of the inverter was revisited during complete circuit testing.

6 Secondary Circuit

The voltage induced on the secondary side planar surface coil is high frequency and varies in magnitude depending on the operating point of the primary circuit. This introduced the need for a secondary side circuit that could rectify the AC power to DC power and regulate the output voltage to 5VDC. The main goals for the secondary circuit were to achieve a high efficiency, be as compact as possible, and minimize the voltage ripple at the output. The initial prototype supplied power through a USB 2.0 connector, however, this was changed to a Micro-B plug in the second design for a reduction in physical size.

6.1 Voltage Rectification

The theory behind full bridge voltage rectifiers is discussed in Section 3.1. The Vishay 2W02G full-bridge rectifier [15] was selected due to its low reverse current of $5\mu\text{A}$, low forward voltage drop of 1.1V per diode, slim profile, and the ability to withstand reverse voltages of up to 200V.

A $180\mu\text{F}$ electrolytic capacitor was selected to limit the voltage ripple at the output of the full bridge rectifier. The value of this capacitor was selected using equations derived for a single-phase full-bridge rectifier with ideal components [4]. Equation 6.1 was used to determine the input voltage magnitude to obtain a specific average DC output voltage.

$$V_m = \frac{V_o * \pi}{2} \quad (6.1)$$

Assuming an output voltage of $V_o = 5\text{V}$, then $V_m = 7.85\text{V}$. Equation 6.2 was used to select a parallel capacitor to limit the output voltage ripple to a specific value.

$$\frac{\Delta V_o}{V_m} = \frac{1}{2fRC} \quad (6.2)$$

An output voltage ripple of 1% was selected, therefore $\Delta V_o = 0.05\text{V}$. At the expected nominal operating point of $f = 100\text{kHz}$, 5V and 1.5A : $R = 3.3\Omega$ and $C = 237.88\mu\text{F}$. A $180\mu\text{F}$ Panasonic 20SEPF180M electrolytic capacitor was selected. The smaller capacitor size was justified due to the Panasonic's significantly slimmer profile compared to other options. It should also be noted the voltage induced on the receiving planar surface coil is actually closer to a square wave, not a perfect sinusoidal waveform as assumed in Equations 6.1 and 6.2.

The square wave is beneficial to producing perfect DC output. Simulations were performed on PLECS using the complete circuit model Appendix B with the reduced capacitor value. Figure 6.1 below shows the output voltage. The maximum and minimum voltages were 5.05V and 4.97V respectively. This yields an output voltage ripple of 1.6% which was in line with the initial design goal of 1%.

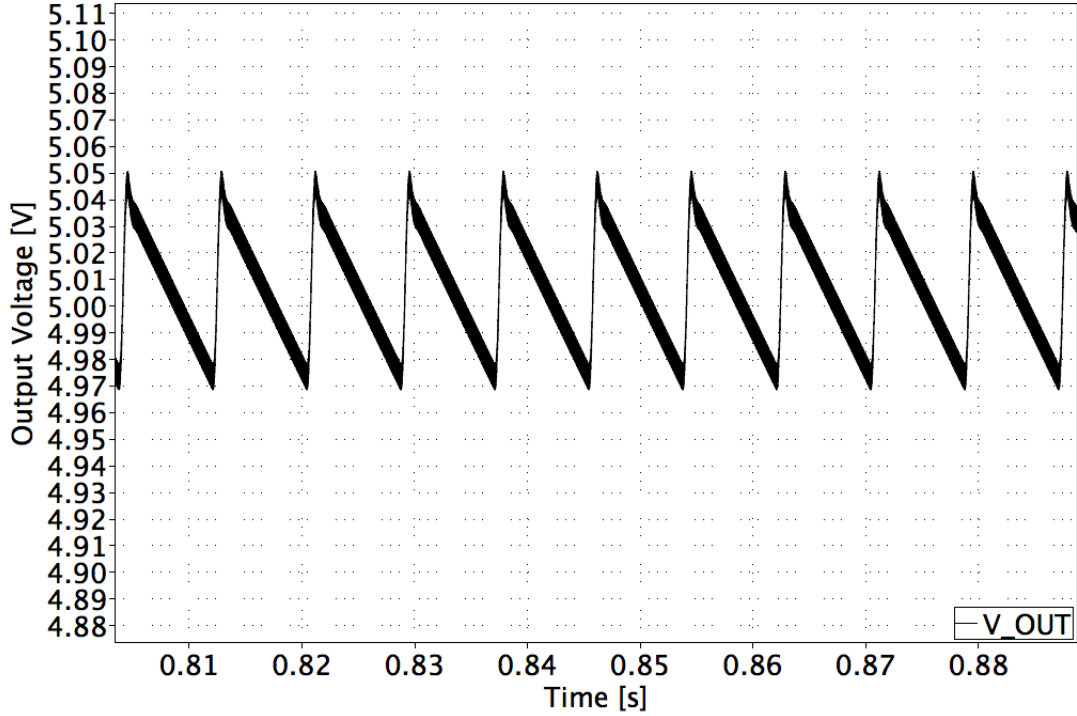


Figure 6.1: Output voltage of full-circuit simulation.

6.2 Voltage Regulation

The standard charging voltage for cell phones is 5VDC with an allowable range from 4.75 - 5.25VDC [16]. To regulate the output voltage to 5V the CUI V7805-2000R non-isolated switching regulator was selected [17]. The technical specifications of the CUI voltage regulator can be found in Table 6.1. Alternative surface mounted options were considered which would have decreased the thickness of the secondary circuit by approximately 3mm. These options required many more supporting passive components with a complicated PCB design while offering no improvement in efficiency. Ultimately the slightly thicker, less expensive, and guaranteed to work option was selected.

Table 6.1: CUI voltage regulator technical specifications [17].

Input Voltage	$6.5 \sim 18V_{DC}$
Output Voltage	$5V_{DC}$
Output Current	2,000mA
Max Voltage Ripple	$45mV_{p-p}$
V_{in-min} efficiency	91%
V_{in-max} efficiency	88%
Voltage Accuracy	$\pm 2\%$
Switching Frequency	340kHz

To limit the voltage ripple at the input and output of the voltage regulator the manufacture recommends to place a $10\mu F$ ceramic capacitor as close to the input pins as possible and a $22\mu F$ ceramic capacitor at the output pins [17]. These recommendations were followed which increased the total shunt capacitance between the rectifier and regulator to $190\mu F$.

The CUI voltage regulator includes over current protection, and thermal shut down. On the other hand, it does not have over voltage protection and the maximum input voltage is 18V. In full circuit simulations, using a small capacitor after the rectifier, large transient voltages were induced upon startup. However, in practice a large capacitor is used, making large voltage transients unlikely to occur. The large capacitor reduced the need for transient over voltage protection, but its inclusion in the design was determined to be an added benefit. This is discussed in detail in Section 6.3.

6.2.1 Input Voltage Requirements

In order for the voltage regulator to operate it requires 6.5VDC at the input [17]. This means there is a minimum AC voltage that must be induced on the secondary side planar surface coils to meet the minimum input requirement of the voltage regulator. Due to calculations in Section 6.1 it is reasonable to assume the shunt capacitor is large enough to keep the rectified voltage at V_M . As mentioned in Section 6.1, the Vishay 2W02G full bridge rectifier has a voltage drop of 1.1V per diode. In each the positive and negative cycles of the input voltage, there are two conducting diodes totalling a 2.2V drop due to rectification. The 6.5V required plus the 2.2V drop across the diodes means the secondary circuit requires a peak voltage of 8.7V to be induced on the secondary side planar surface coil. The calculated value was confirmed in simulation, and eventually testing which is discussed in Section 6.5.

6.3 Transient Voltage Suppression

As mentioned in 6.2 over voltage scenarios are unlikely but possible, therefore over voltage protection was required. Since the over voltages observed in the simulation were purely transient, a Transient Voltage Suppression (TVS) diode was selected. A unidirectional TVS diode appears as an open circuit until the reverse standoff voltage is reached. Once the reverse standoff voltage is reached, the diode breaks down and acts as a short circuit. The short circuit provides a path for the extra energy preventing damage to the protected device. Further information on the application of TVS diodes can be found in the article *What Are TVS Diodes?* by Semtech Corporation [18].

The Micro Commerical Components P4KE20A was selected because of its 17.1V reverse standoff voltage and low reverse leakage current of $1\mu\text{A}$ [19]. This will assure protection for the voltage rectifier which has a maximum input voltage of 18V, while only consuming microwatts of power in normal operation.

6.4 Phone Integration

USB ports have become the standard for Portable Devices (PD) charging. USB charging makes use of four pins: positive and negative power pins, and positive and negative data pins. A Dedicated Charging Port (DCP), as defined by the standard for Battery Charging Specifications, is a “downstream port on a device that outputs power through a USB connector, but is not capable of enumerating a downstream device” [16]. The PD is able to recognize the presence of a DCP by configuring the port as shown in Figure 6.2. Table 6.2 shows the standardized technical specifications of the DCP. Since there is no maximum value for R_{DAT_LKG} it was justified to not include these resistors in efforts to save space. R_{DCP_DAT} was selected to be the maximum value of 200Ω . The maximum value was selected to limit the current in the portable device in the case of a data pin voltage mismatch. The successful recognition of a DCP by the cellular device was confirmed and is shown in Section 8.

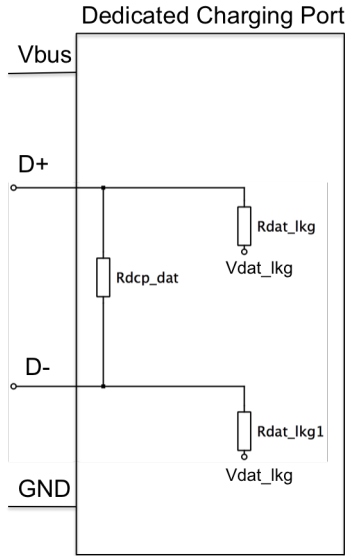


Figure 6.2: Dedicated charging port diagram.

Table 6.2: Dedicated charging port specifications [16].

Parameter	Symbol	Min	Max	Units
Charging Port Output Voltage	V_{CHG}	4.75	5.25	V
Allowed PD Current Draw from Charging Port	I_{DEV_CHG}		1.5	A
DCP Resistance Across D±	R_{DCP_DAT}		200	Ω
Data Line Leakage Resistances	R_{DAT_LKG}	300		$k\Omega$

It was determined that for the first prototype a USB 2.0 port would be the most universal output for testing purposes, as it would be able to interface USB chargeable device. By using a USB port it would also be possible to use a USB power meter that would be able to accurately measure the output power.

The downside of the USB port was its large physical size. It would require a shortened USB cable to be plugged into the cellular device. This would consume a considerable amount of space in the cellphone case. To resolve this issue it was determined that the voltage regulator would output directly to a Micro-B plug. To implement this design, a standard Micro-B cable was cut and the power lines were connected directly to the output of the voltage regulator, the data lines were shorted with a 200Ω resistor.

6.5 Implementation

Upon receiving all components, the circuit was assembled on perforated circuit board. Assuming a maximum current of 2A, number 16 wire gauge was selected using the American Wire Gauge chart. The circuit was tested using a signal generator under no load conditions. A sinusoidal signal was applied to the input and tested for frequencies ranging from 50kHz to 200kHz. Starting from a magnitude of 0.1VAC the voltage was slowly increased and the output was monitored. For all frequencies, the output was 0VDC until the input magnitude reached 8.6VAC at which point the output was 5VDC as shown in Figure 6.3. The start-up voltage of the regulator at 8.6V agreed with both the calculated and simulated values. The circuit maintained a 5VDC output for input voltages ranging from 8.6-10VAC. Accurate output voltage ripple calculations were not performed due to large amounts of noise on the oscilloscope.

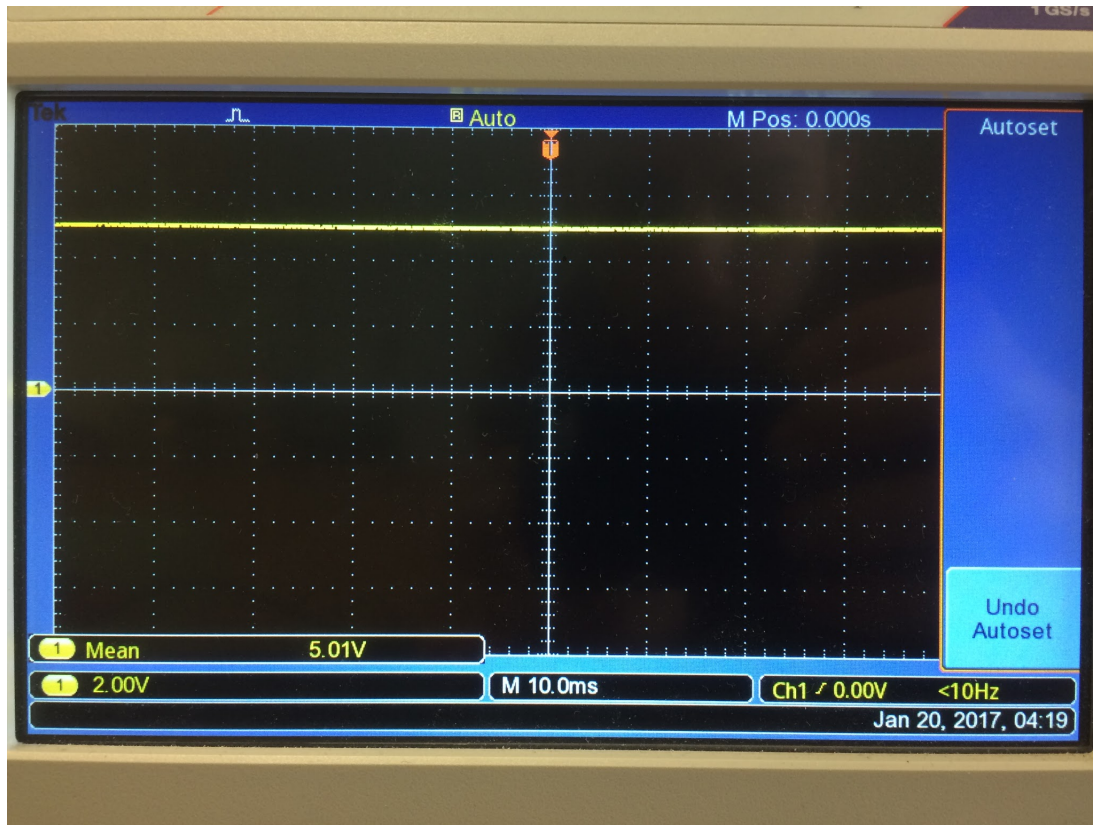


Figure 6.3: Secondary circuit output under no-load conditions with signal generator input.

7 Case Design

Seamless integration of the wireless charging circuitry was the prerequisite to designing a custom charging platform and cellphone case. The designs were approached with an emphasis on minimizing overall profile to preserve functionality.

7.1 Design Considerations

Aesthetics were a major consideration during design of the cell-phone charging pad. A sleek and simple approach was taken to provide a clean look that is similar to other wireless chargers currently on the market. The charging pad size was carefully designed to be comparable with the cellphone case dimensions and to ensure sufficient room for primary electronics. To help with overall project efficiency, coil alignment was considered during the design stage. Edges were created to aid in self alignment of the coils if the user were to place the phone slightly off center of the charging pad. A cavity in the top face of the charging pad was included reduce the overall distance between the primary and secondary coils. Additionally, a very thin screen was used to cover the primary coil and further reduce the distance between coupled coils. To ensure functionality of the cell-phone detection module, the maximum detection distance of 2cm had to be respected. The RFID sensor was mounted on the roof of the case in line with the RFID tag in the phone case. The charging pad was designed in two pieces, a bottom plate and a shell. The primary side electronics are mounted on the bottom plate and the shell of the charging pad covers the electronics from view. The two pieces were assembled with screws so that they remain removable if the charging pad ever requires repair.

Minimizing the overall size was the primary concern in the design of the cellphone case. To maintain a low profile, a cavity was placed in close proximity to the USB port at the bottom end of the cellphone. This reduced the length of wiring from the voltage regulator to the USB port. The receiving coils were placed adjacent to the RFID tag along the backside of the case, rather than placing them atop one another. This was in an effort to reduce the overall thickness of the case, but had the added benefit of minimizing the potential of interference between the RFID tag and secondary coils. It was essential that all peripheral buttons and ports of the device remain functional, thus access to these peripherals was maintained in the case design.

7.2 Implementation

Once an initial design of the charging pad was developed in Fusion 360TM 3D CAD software, it was sent for review. Suggestions for changes were given due to the 3D printing process. Considerations such as thickness of material, largest possible angles, accuracy of the 3D printer caused minor changes to the design to improve the printing process. The design was sent to the 3D printing shop at the University of Manitoba for fabrication.

Two preliminary cellphone case designs were created, in Fusion 360TM, and printed in the Engineering Tech Shop in a hard plastic material. This provided a cost effective method of ensuring that all dimensions were correct, but would not be practical as a final product as its lack of malleability made it difficult to attach to the phone and provided very little shock absorption. The final printing was completed in a semi-flexible compound, PETG Plastic. The finalized CAD design of this case is illustrated in Figure 7.1.

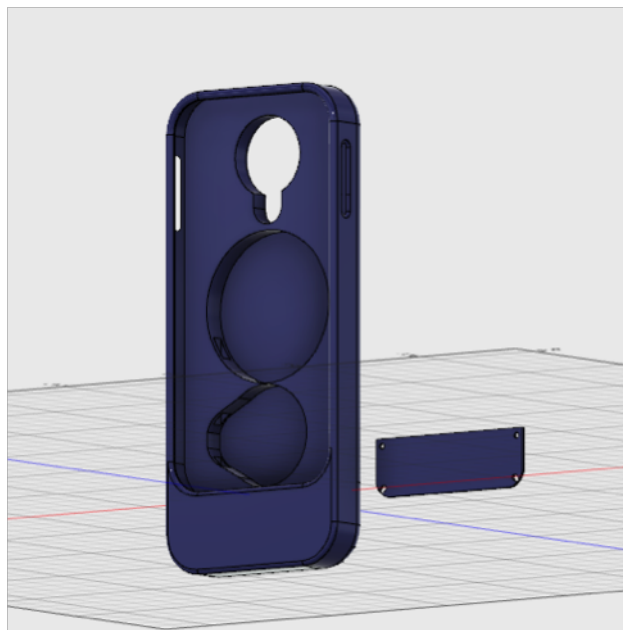


Figure 7.1: 3D Model of phone case.

8 Final Design

The complete circuit was initially tested using a resistive load for its pure power transferring capabilities. The maximum recorded efficiency was 36% at a frequency of 33kHz with a coupling coefficient of 0.8. At this efficiency, the output voltage was 5VDC and the current was 1.5A. The primary and secondary circuits were then mounted in their respective cases. A Samsung Galaxy S4 was the phone selected to test practical operation of the circuit

and RFID interfacing. The Ampere App by Braintrapp, available in Google Play, was used to measure the charging current [20]. The wireless charger successfully charged the test phone with a net current of 1200mA as shown in Figure 8.1.



Figure 8.1: Successful wireless charging at 1200mA.

8.1 System Integration

All system subsections, with the exception of the inverter, were previously tested individually. Since the inverter design was dependant on the other subsections, the inverter testing was incorporated into the system integration. This process began by connecting the source AC-DC converter to the inverter board and the Arduino. The converter provided adequate power to the Arduino and the supporting circuitry of the inverter. Interfacing between the Arduino and inverter consisted of three wires; the 5V source pin and two I/O pins. The inverter was successfully able to supply high frequency power when the primary coil was connected. The secondary coil was then attached at the input of the functional secondary AC-DC converter. A Micro-B cable connected the secondary circuit output to the phone. Coupling the coils completed the circuit as illustrated in figures 8.2 and 8.3.

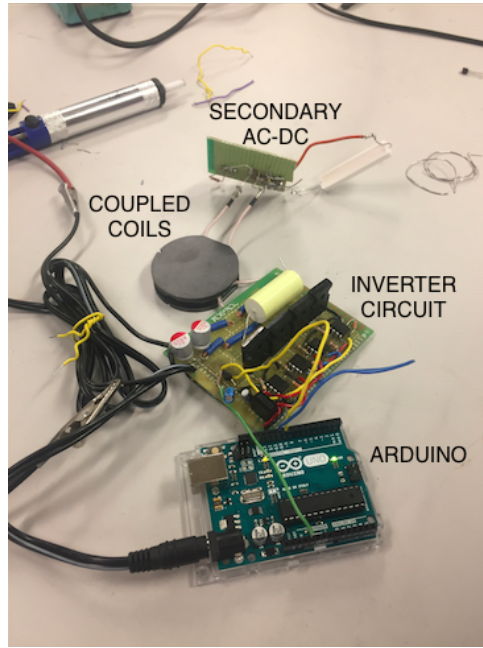


Figure 8.2: Implemented system with 3.3Ω load.



Figure 8.3: Implemented system successfully charging a Samsung Galaxy S4.

The initial project budget was estimated to be \$435.95, excluding a 14% project contingency. The project was completed under budget, with an actual cost of \$363.22 and 0% of the contingency used. A detailed comparison of the original budget versus actual cost can be found in Appendix D.

8.2 Operation Results

The complete circuit was tested with a coupling coefficient of 0.8 (no air gap) and a coupling coefficient of 0.6 (2mm air gap). A 3.3Ω , 10W resistor was used to simulate the maximum power draw of a cellular device. The input current was measured by placing an ammeter in series with the hot wire output of the AC-DC power supply and output voltage was measured across the resistive load. The frequency and duty cycle of the inverter were varied to find an optimal operating point with regard to efficiency. This was calculated using Equations 8.1-8.3 and the results are summarized in Tables 8.1 and 8.2.

$$P_{in} = I_{DC} * V_{in} \quad (8.1)$$

$$P_{out} = \frac{V_{out}^2}{3.3} \quad (8.2)$$

$$\eta = \frac{P_{out}}{P_{in}} \quad (8.3)$$

Table 8.1: Efficiency results with coupling coefficient of 0.8.

0.8 Coupling						
Frequency (kHz)	Duty Cycle (%)	Input Current (A)	Input Power (W)	Output Voltage (V)	Output Power (W)	Efficiency (%)
21	30%	1	12	3.6	3.93	33%
27	30%	1.2	14.4	3.9	4.61	32%
31	30%	1.6	19.2	4.6	6.41	33%
31	36%	1.5	18	4.5	6.14	34%
32.5	32%	1.7	20.4	4.9	7.28	36%
32.5	34%	1.7	20.4	4.8	6.98	34%
33	30%	1.77	21.24	4.99	7.55	36%
33	26%	1.7	20.4	4.8	6.98	34%
110	20%	1.1	13.2	2.7	2.21	17%
115	21%	1.9	22.8	4.2	5.35	23%
115	25%	1.8	21.6	4	4.85	22%
135	25%	1.4	16.8	3.2	3.1	18%
160	25%	1.07	12.84	2.5	1.89	15%

Table 8.2: Efficiency results with coupling coefficient of 0.6.

0.6 Coupling						
Frequency (kHz)	Duty (%)	Input Current (A)	Input Power (W)	Output Voltage (V)	Output Power (W)	Efficiency (%)
39	28%	1.6	19.2	4.2	5.35	28%
39	24%	1.8	21.6	4.8	6.98	32%
38	20%	1.85	22.2	4.99	7.55	34%

8.3 Analysis of Results

It can be seen in Tables 8.1 and 8.2 that by varying the input parameters an optimized operating point can be found. By varying the frequency it is possible to achieve a suitable output voltage, and by varying the duty cycle it is possible to maximize the efficiency.

8.3.1 Achievement of Specifications

System integration revealed that three out of the four original specifications were met as shown in Table 8.3. The wireless charger uses mains voltage to supply all of its components. Test results of Tables 8.1 and 8.2 demonstrate that the charger was able to supply 1.5A at 5V for 7.5W. The phone successfully recognized the presence of a DCP by drawing a net 1200mA into the battery. For comparison, this is identical to the factory wall charger provided with the phone. The background current drawn from the battery was 460mA and was included in this net calculation by the app. The only specification not met was the efficiency; the maximum nominal efficiency was 36%.

Table 8.3: Achieved project specifications.

Performance Metric	Target Value	Achieved	Pass/Fail
Input Voltage	120VAC, 60Hz	120VAC, 60Hz	Pass
Output Voltage	5VDC Nominal, 4.75-5.25VDC Range	5VDC $\pm 2\%$	Pass
Output Current	0.5 - 1.5A	0.5 - 1.5A	Pass
Efficiency	55% Nominal Max	36%	Fail

8.3.2 Efficiency Analysis

To understand why the efficiency target of 55% was not achieved, the initial estimate was reconsidered. The proposed efficiency was calculated by looking at each indi-

vidual circuit subsection, estimating its appropriate efficiency, and obtaining the cascaded efficiency.

The VSK-S20-24V-T model converter, rated for 20W with an efficiency of 85%, was used to estimate the AC-DC converter efficiency [21]. The SCI15 inverter was used for the inverter efficiency estimate, as it was the only inverter with a data sheet specifying efficiency. It is rated for 1500W and has an efficiency of 93% [22]. Since efficiency increases with power, an estimate of 85% was chosen for this subsection. Simulations of the coupled coils showed that an efficiency of 90% was attainable. The secondary AC-DC converter efficiency was estimated to be identical to the primary AC-DC converter, at 85%. Efficiency of the secondary side voltage regulator was estimated to be 90%, based on the PI3424-00-LGIZ model regulator [23]. Based on the above estimates the overall circuit efficiency was calculated to be 55%. This is in agreement with the maximum efficiency of 57% achieved in Choi's paper [1].

The estimates explained above overlooked two important details which made the initial efficiency estimate unattainable. First, the final operating frequency of the inverter was on the lower side of the resonance peak. Contrary to design simulations, the measured efficiency at higher frequencies was worse. The presence of parasitics and non dedicated circuit components contributed to the non-optimal operation of the inverter. As per the second simulation shown in Section 5.3.2, the combined inverter and coil efficiency at a lower frequency can be estimated to be 63%, much lower the initial estimate of $90\% * 90\% = 81\%$. The secondary rectifier efficiency estimate of 85% also proved to be unrealistic. This was due to the 1.1V drop per conducting diode of the full bridge rectifier. With this voltage drop, the maximum efficiency possible is 74%. The calculation to determine this value can be found in Appendix E.

In addition to the previous oversights, the reference efficiency of 57% did not actually include the input AC-DC converter. Had this been noticed in the beginning, it would have alerted that the target of 55% was not realistic.

Using the two new efficiency estimates, an adjusted target system efficiency could be calculated. It should also be noted that the input current was measured after the primary rectification due to safety concerns and thus the calculation was made without the input AC-DC efficiency. Using the more realistic values, the adjusted efficiency estimate was 42%. However, the measured efficiency still did not meet the target. Additional losses not accounted for include the Arduino and gate driver supply currents, which were not considered in the proposal stage.

9 Future Considerations

The circuit that was designed and built proved to be able to transfer power wirelessly to the cellular device. In order to achieve the specified efficiency, some steps could be taken to improve the design. Both the inverter and the secondary circuit could be fabricated on PCB allowing for cleaner circuit paths and improved heat conduction. The isolated traces of a PCB would mitigate parasitic capacitances that impacted the operation of the circuit at frequencies above the resonance peak. Lowering the temperature of the components would allow for better overall conduction. Additionally, with a PCB, surface mount components could be used. During initial research, it was observed that surface mount components were generally more efficient. With a more efficient rectifier and voltage regulator, the limiting factor on power transfer to the secondary load becomes the voltage induced on the coil instead of power loss through AC-DC conversion.

The availability of components during building and testing limited the ability to procure parts more suitable to the application. Using inverter switches that are rated for less power, but are quicker, would increase performance of the circuit at frequencies above the resonance peak. With more suitable switching components, the limiting factor on operating frequency of the inverter becomes the inductive load as opposed to the switches.

10 Conclusion

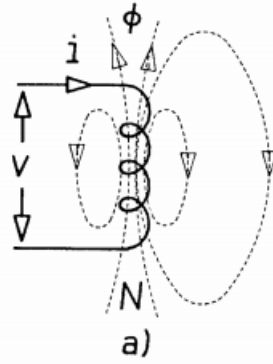
The Design and Implementation of a Wireless Cellphone Charger was completed and has been outlined in the preceding report. Design considerations and choices were explored with respect to each sub-circuit. Simulation of the sub-circuits were analyzed to justify proceeding with a prototype. Physical construction of the circuits, including part selection was explained. Integration of each sub-circuit into the complete system and testing of the complete circuit was summarized.

Four project specifications were outlined: input voltage, output voltage, output current and efficiency. Testing revealed that the circuit met all specifications with the exception of efficiency. Explanation was provided for why the circuit failed to meet the efficiency goal. Future considerations were suggested to improve efficiency and meet all performance metrics in future designs.

In the final build, the primary electronics were housed in a 3D printed charging pad and the secondary electronics were housed in a 3D printed phone case. An RFID circuit between the pad and the phone case controlled operation of the charger. During the absence of the phone, the inverter did not operate and no power was output. In the presence of the phone, the circuit would be completed and the phone would successfully charge.

Appendix A - Coil Model Derivation

To begin the derivation of the planar surface coil equivalent model, a single coil was first considered as shown below.



The voltage of the coil is related to the flux through the coil by the following equation:

$$v = N \left(\frac{d\phi}{dt} \right) \quad (10.1)$$

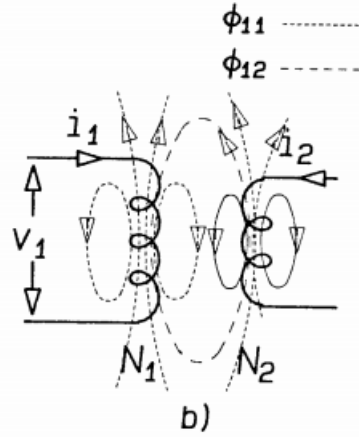
Since the inductance of a coil is defined as:

$$L = \frac{N\phi}{i} \quad (10.2)$$

The voltage of the inductor can be expressed in terms of current:

$$v = L \left(\frac{di}{dt} \right) \quad (10.3)$$

Which is just the voltage current relationship of an inductor. Next, consider two nearby coils as shown below.



With the presence of the second coil, the voltage of the first coil is determined not only by its own flux but also the flux of the second coil. In the previous figure, ϕ_{11} is the flux inside coil 1 due to current i_1 and ϕ_{12} is the flux inside coil 1 due to current i_2 . The new equation for the voltage of coil 1 must include these two contributions to the total flux:

$$v_1 = N_1 \left(\frac{d\phi_{11}}{dt} \right) + N_1 \left(\frac{d\phi_{12}}{dt} \right) \quad (10.4)$$

By defining the self inductance and the mutual inductance:

$$L_{11} = \frac{N_1 \phi_{11}}{i_1} \quad (10.5)$$

$$L_{12} = \frac{N_1 \phi_{12}}{i_2} \quad (10.6)$$

We can rewrite the voltage as:

$$v_1 = L_{11} \left(\frac{di_1}{dt} \right) + L_{12} \left(\frac{di_2}{dt} \right) \quad (10.7)$$

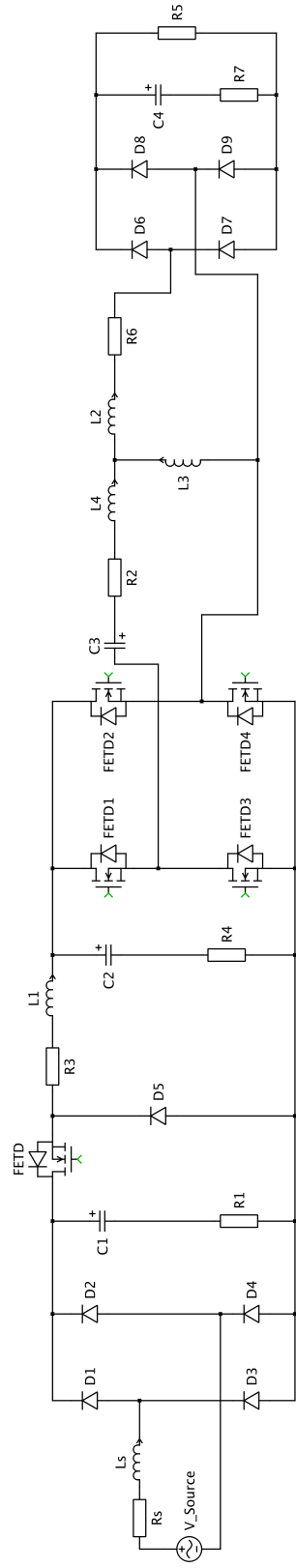
L_{12} and the equivalent for the second coil, L_{21} , are equal to each other and they are usually written as L_M . The voltage equation can be rewritten as:

$$v_1 = (L_{11} - L_M) \left(\frac{di_1}{dt} \right) + L_M \left(\frac{d(i_1 + i_2)}{dt} \right) \quad (10.8)$$

$$v_2 = (L_{22} - L_M) \left(\frac{di_2}{dt} \right) + L_M \left(\frac{d(i_1 + i_2)}{dt} \right) \quad (10.9)$$

The above equations can be used to create an equivalent circuit model for coupled inductors, which is shown in Figure 2.1 on Page 3.

Appendix B - Complete Circuit



Appendix C - Arduino Code

```
#include <SPI.h>
#include <MFRC522.h> //Include RFID Library
#include <PWM.h> //Include PWM Library

//*****
//Definitions*****
//*****

int duty = 80; //duty cycle
int32_t frequency = 35000; //frequency (in Hz) of all PWM pins

#define RST_PIN 4 // Configurable, see typical pin layout above
#define SS_PIN 5 // Configurable, see typical pin layout above
#define idleLED 3 //LED to indicate absense of device

#define switchAC 6 //Control switch a and c of inverter

String read_rfid;
String pswdOk = "39bb5a9e";

//*****


MFRC522 mfrc522(SS_PIN, RST_PIN); // Create MFRC522 instance
int count = 0; //keep count of indicator light

void setup()
{
    digitalWrite(9, LOW);
    digitalWrite(10,LOW);
    pinMode(idleLED, OUTPUT);
    pinMode(switchAC, OUTPUT);
    //digitalWrite(9, LOW);
    //digitalWrite(10,LOW);
    Serial.begin(9600); // Initialize serial communications with the PC
    while (!Serial); // Do nothing if no serial port is opened...
    (added for Arduinos based on ATMEGA32U4)
    SPI.begin(); // Init SPI bus
    mfrc522.PCD_Init(); // Init MFRC522
    Serial.println(F("Scan PICC to see UID, SAK, type, and data blocks..."));
    //delay(5000);
}
```

```

void loop() //Main Method
{
    if ( ! mfrc522.PICC_IsNewCardPresent() ) //Search for any cards
    {
        digitalWrite(9, LOW);
        digitalWrite(10,LOW);
        digitalWrite(idleLED, HIGH);
        delay(500);
        digitalWrite(idleLED, LOW);
        delay(2000);
        return;
    }

    if ( ! mfrc522.PICC_ReadCardSerial() ) //Search for recognizable cards
    {
        return;
    }

    dump_byte_array(mfrc522.uid.uidByte, mfrc522.uid.size);...
    //Determine rfid code
    Serial.println(read_rfid); //for visualization print rfid code to console

    if(read_rfid == pswdOk) //If code is expected code then begin charging
    {
        digitalWrite(switchAC, HIGH);
        Serial.println(pswdOk);
        setPWM(frequency, duty);
        detected();
        digitalWrite(9, LOW);
        digitalWrite(10,LOW);
        digitalWrite(switchAC, LOW);
    }
}

void dump_byte_array(byte *buffer, byte bufferSize)...
//Method to extract rfid code
{
    read_rfid="";
    for (byte i = 0; i < bufferSize; i++)
    {
        read_rfid = read_rfid + String(buffer[i], HEX);
    }
}

void detected() //Method to indicate rfid was detected
{
    while (read_rfid == pswdOk) //As long as rfid tag is...
}

```

```

    present continue charging
{
    delay(500);
    if(!mfrc522.PICC_ReadCardSerial()) {
        mfrc522.PCD_Init();
        if(!mfrc522.PICC_IsNewCardPresent()) {
            return;
        }
    }
}

void setPWM(int32_t frequency, int duty) //method to set frequency...
and duty cycle of pwm pins 9 and 10
{
    InitTimersSafe(); //Initializes all timers except timer0
    SetPinFrequencySafe(9, frequency); //Set pin 10 to frequency [Hz]
    SetPinFrequencySafe(10, frequency); //Set pin 5 to frequency [Hz]

    pinMode(10,OUTPUT);
    digitalWrite(10,LOW);

    int x = map(duty, 0, 100, 0, 256);
    int y = map(100-duty, 0, 100, 0, 256);
    pwmWrite(9,x); //Set duty cycle of pin 9 to duty
    delay(1000);
    pwmWrite(10,y); //Set duty cycle of pin 10 to 100-duty
}

```

Appendix D - Budget

Original Budget			Actual Cost		
Function	Description	Cost	Function	Description	Cost
Software	AutoCAD PLECS Altium	\$0.00	Software	Autodesk Fusion360 PLECS	\$0.00
Electrical Components	Diodes Capacitors Resistors Household plug Wire/cable Micro USB Cable Connection Hardware EM Shield Switches	\$55.00	Electrical Components	TVS Diode Capacitors Power Resistors Household Plug Wire/Cable Micro USB Cable Connection Hardware EM Shield	\$143.94
				Inverter Switches Pulse Transformer Inverter Cricuit Gate Driver NAND Chip DC-DC Converter	
Packaging	Charging station Phone case	\$30.00 \$20.00	Packaging	Charging station Phone case	\$0.00 \$28.28
Controller	Arduino Uno	\$35.95	Controller	Arduino Uno Current Sensor	\$65.25
Coil Design	PCB Coils	\$210.00	Coil Design	Coils	\$61.72
Secondary AC-DC	PCB Design	\$35.00	Secondary AC-DC	Voltage Regulator USB Receptacle Heat Sink Bridge Rectifier	\$19.95
Two Step AC-DC Conv.	TBD	\$50.00	Two Step Ac-DC Converter	20 W Desktop Power Supply	\$44.08
Budgeted Total \$435.95			Actual Total \$363.22		
Project Contingency	14%	\$61.03	Project Contingency	0%	\$0.00
Advisor Additional Funding	If required	N/A	Advisor Additional Funding	Not Required	N/A
Overall Budgeted Total \$496.98			Actual Cost \$363.22		

Appendix E - Secondary Circuit Rectifier Efficiency

The maximum circuit efficiency for the secondary side full circuit rectifier can be calculated from the equations below. Assuming a 7.5W load and a worst case 6.5VDC at the input to the voltage regulator, the current through the full wave diode bridge can be calculated as:

$$I_{DC} = \frac{7.5W}{6.5A} = 1.154A \quad (10.10)$$

Due to the 1.1V drop across each conducting diode, the power lost to the full wave rectifier can be calculated as:

$$P_{loss} = 2.2V * 1.154A = 2.31W \quad (10.11)$$

The efficiency of the voltage rectifier can therefore be calculated as:

$$\eta = \frac{P_{out}}{P_{out} + P_{loss}} = 76.4\% \quad (10.12)$$

References

- [1] Byungcho Choi *et al.* Design and implementation of low-profile contactless battery charger using planar printed circuit board windings as energy transfer device. *IEEE Transactions on Industrial Electronics*, 51(1):140–147, February 2004.
- [2] Zhe Zhang. *Coupled Inductor Magnetics in Power Electronics*. PhD thesis, CIT, Pasadena, CA, 1987. Ph.D. dissertation.
- [3] Wurth Elektronik. *WE-WPCC Wireless Power Charging Transmitter Coil Datasheet*, December 2015.
- [4] Daniel W. Hart. *Power Electronics*. McGraw-Hill Education, 1221 Avenue of the Americas, New York, NY 10020, Jan. 2010. ch. 4, 6, and 8.
- [5] Inventus Power. *IPD20 Series Class 1 20 Watt ITE Desktop Power Supply*, 2016. Datasheet.
- [6] NXP Semiconductors N.V. *MFRC522 Datasheet*, April 2016.
- [7] Miguel Balboa. Arduino rfid library for mfrc522, January 2012. Computer Code.
- [8] Atmel. *ATmega328/P*, November 2016.
- [9] Sam Knight. arduino-pwm-frequency-library, 2012. Computer Code.
- [10] Kenneth C. Smith Adel S. Kendra. *Microelectronic Circuits*. Oxford University Press, 6th edition, 2009. ch, 4.
- [11] S.O. Kasap. *Principles of Electronic Materials and Devices*. McGraw-Hill Education, 3rd edition, 2001.
- [12] L. Wuidart B. Maurice. Drive circuits for power mosfets and igbts. Technical report, STMicroelectronics, 1999.
- [13] International Rectifier, 233 Kansas St., El Segundo, California 90245 USA. *IRFP250NPbF HEXFET®Power MOSFET Datasheet*, August 2010.
- [14] Avago Technologies. *HCPL-3180 Gate Drive Optocoupler Datasheet*, March 2009.
- [15] Vishay. *Glass Passivated Single-Phase Bridge Rectifier*, June 2016. W20G2 Datasheet.
- [16] Mark Lai *et al.* Battery charging specification. Technical report, Allion Test Labs, December 2010. Revision 1.2.
- [17] CUI Inc. *V78-2000 Series Datasheet*, March 2014. Non-isolated Switching Regulator.
- [18] Semtech. *What Are TVS Diodes?*, 9th edition, 2000. TVS Diode Application.

- [19] Micro Commercial Components. *P4KE20A Datasheet*, July 2013.
- [20] Braintrapp. Ampere. App, January 2017. Available in Google Play.
- [21] CUI INC. *VSK-S20-T Datasheet*, November 2015. AC-DC Power Supply.
- [22] InifiSolar. *2KW3KW Hybrid PV Inverter User Manual*, 2.1 edition, 2016.
- [23] Vicor. *PI34xx-00 Cool-Power ZVS Buck Regulator Datasheet*, 1.3 edition, December 2015.